Where are the limits of Mesozoic intracontinental sedimentary basins of southern France?

J. Barbarand, P. Préhaud, François Baudin, Y. Missenard, J.M. Matray, T. François, T. Blaise, R. Pinna-Jamme, C. Gautheron

Where are the limits of Mesozoic intracontinental sedimentary basins of southern France?

Barbarand J.[1,*], Préhaud P.[1], Baudin F.[2], Missenard Y.[1], Matray J.M.[3], François T.[1], Blaise T.[1], Pinna-Jamme R.[1], Gautheron C.[1]

[1] Université Paris-Saclay, CNRS, GEOPS, Orsay, 91405, France.

[2] Sorbonne Université and CNRS, UMR 7193 ISTeP, 4 place Jussieu 75005 Paris, France

[3] IRSN, 31 avenue de la Division Leclerc, BP 17 92262 Fontenay-aux-Roses Cedex, France

Abstract

Reconstitution of the geometry of sedimentary basins is fundamental to understand the nature of present sedimentary rocks and the economic potential in hydrocarbon and mineral resources. Present-day topography of southern France shows elevations growing between the Meso-Cenozoic Aquitaine Basin to the South-East Basin across the Variscan domain and the Jurassic Causses small basin with maximum relief in the Cévennes area. Present-day elevation offset is of approximately 1000 m. This geometry questions the paleogeography and dynamics of these various domains and the relative elevation of the Variscan domain during the subsidence of adjacent Aquitaine and South-East Basins. In this study, we investigate the geological history of the Variscan basement high and the Causses small basin using paleotemperatures deduced from organic matter analysis, low temperature thermochronology and regional geological constraints.

Lower Jurassic (upper Pliensbachian and Toarcian) marls sampled across the area from the Aquitaine Basin to the South-East Basin have similar depositional environments containing mainly type III oganic matter, and close Tmax values ranging between 430 and 440±2°C. These data show that the entire south Massif Central has undergone a similar burial history. considering that these values are explained by burial. Low temperature thermochronology data have been acquired on basement rocks outcropping on the borders of sedimentary basins (Rouergue, Cévennes and Margeride). Fission-track ages are ranging between 74±5 and 187±6 Ma and track lengths between 11.5±0.3 and 13.6±0.1 µm; apatite (U-Th)/He corrected ages are ranging between 65±5 and 184±15 Ma. Data inversion with the software QTQt indicates a

cooling episode starting at the end of Early Cretaceous or beginning of Late Cretaceous from maximum temperature of 100±10°C in the Rouergue and Cévennes area and from 80±10°C in most of the Margeride area.

Thermal indicators are compatible with the erosion of a Middle/Upper Jurassic and Cretaceous sedimentary cover of 1400±400 m assuming a thermal paleogradient of 35°C/km. The preserved sedimentary cover attests of a Middle and Upper Jurassic – Lower Cretaceous sedimentary cover of 1000 to 2000m in the Aquitaine and South-East basins. This erosion phase occurred during mid-Cretaceous and is associated to a major geodynamical event characterized by large amplitude (from the Aquitaine Basin to Durancian doming in the South-East Basin) and by kilometric offset. We interpret also these data to show that marine connections have existed between the Aquitaine Basin and the South-East Basin during the Jurassic and likely Early Cretaceous. The present-day morphology of the area has then been acquired after Cretaceous times and may result from the Pyrenean orogenic event during Eocene times.

INTRODUCTION

Sedimentary basins represent archives to unravel the Earth history including sedimentary environments, paleoclimates, paleogeography and geodynamics (Einsele, 2000). Understanding of these parameters is based mainly on the present-day distribution of sedimentary deposits including thickness, structural context and surface distribution. The role of post-sedimentary processes affecting the rocks including erosion is also important as present-day distribution and preserved sedimentary series do not necessarily represent the initial sedimentary basin geometry. Defining the evolution of sedimentary basins and considering erosion are also important for resource evaluation as the interface between basement and sedimentary cover might be enriched in metals (Boiron et al., 2010) and the hydrocarbon potential is highly controlled by the depths reached by source rocks. Quantifying erosion can be achieved using sedimentary balance with the well-developed source to sink approach (Romans et al., 2016), but this approach is tedious when working on old archives where several episodes of erosion might exist and is challenging when considering the erosion of carbonate rocks. In such situations, erosion can be deduced from thermal history reconstruction from organic matter and low temperature thermochronology.

The southern France represents an interesting area to investigate the former extent of sedimentary. Located on the stable European platform, it represents an intraplate domain where little deformations occurred. Present-day topography shows a clear contrast between elevated basement area, the Variscan French Massif Central (Margeride, Rouergue, Cévennes), clear of sediments and the small Jurassic Causses Basin in central position and Meso-Cenozoic sedimentary basins located at lower elevation including the Aquitaine Basin in the west and the South-East Basin in the east (Fig. 1A). At first sight, this suggests a relative stability of the region with sedimentary rocks deposited at the edge of the basement. Nevertheless, remnants of Jurassic sedimentary cover lying on the basement questions whether this basement may also have been subsiding at that time and after.

Contacts between the South-East and Aquitaine basins and the basement correspond to significant faults (respectively Cévennes Fault and Sillon Houiller) which have been active since Paleozoic times. The Cévennes Fault characterizes today a rapid change in elevation, the basin being much lower than the basement (Fig. 1A and 1B). Such geometry and the absence of a thick sedimentary cover suggest that the basement was at high elevation early on. Sediment facies analysis does not allow to constrain the former extent of the basin but Triassic sandstones and

Lower Jurassic limestones resting unconformably on the basement at high elevation (>1000m) and indications of Cretaceous limestones in karstic formation in the south of the Causses Basin (Alabouvette et al., 1984; Bruxelles et al., 1999) suggest that the South-East Mesozoic sedimentary cover may have extended farther on the basement. In the Aquitaine Basin, transition between the sedimentary realm and the basement is much smoother (low contrast in elevation) but the presence of the Sillon Houiller and the progressive decrease of the thickness of the sedimentary section towards the basement have make people consider that a clear limit existed between these two domains. (Simon-Coinçon et al., 1997; Biteau et al., 2006)

The objectives of this study are to question the Meso-Cenozoic evolution of the basement high and adjacent sedimentary basins limits. We use two complementary thermal indicators, organic matter and low temperature thermochronology (fission-tracks and (U-Th-Sm)/He on apatite crystals) and regional geology correlations to reconstruct the thermal history and thus the former geometry of the south of the French Massif Central and determine the amount and the age of potential erosion phases.

GEOLOGICAL CONTEXT

The studied area is located at a crossroad of several geological structures (Fig. 1B). It corresponds to the south of the Massif Central, a segment of the Variscan orogen deformed during Carboniferous (Faure et al., 2009). It results from an assemblage of metamorphic, magmatic and sedimentary rocks which form today the basement of the Massif Central. Major faults have structured the area including the Sillon Houiller Fault to the west and the Cévennes Fault to the east. Late deformation of the massif is recorded by intramontaneous sedimentary basins filled with Stephanian to Permian sediments (Blès et al 1989).

The studied area then underwent an episode of extension, associated to the break-up of Pangea, lasting from the late Permian until the Middle Jurassic. This episode led to the formation of two large basins preserved on the western and eastern part: the Aquitaine Basin and the South-East Basin. Sedimentation went on during Mesozoic with the deposition of thick sedimentary sequences (up to ~10 km, Curnelle and Dubois, 1986).

In the south of the Massif Central, the Causses area represented during the Early Jurassic a large epeiric carbonate platform located on the passive margin of the South-East Basin and was

affected from Hettangian to Toarcian times by tectonic extension (Baudrimont and Dubois, 1977). Inherited basement faults formed during the Variscan orogeny were reactivated as synsedimentary normal faults. During Mesozoic time, the Causses domain is thought to be connected to the South-East basin by the Cévennes High and to the Aquitaine Basin by the Rodez Strait (Figure 1B). This period is characterized by a continuous sedimentation over the South of the Massif Central, including Variscan basement. Jurassic sedimentary rocks close to the Aquitaine and South-East basin boundaries and in the Causses domain are characteristics of shallow carbonate platform with marine environments (Dubois, 1985; Bonijoly et al., 1996; Biteau et al., 2006). Jurassic series outcropping close to the basement are characterized by low bathymetry that makes some authors assume that shoreline was close (Ciszak et al., 1999). On the other hand, such low bathymetry facies are widespread in the Jurassic series, even in the center of the Causses basin: during Late Hettangian to Sinemurian, deposits correspond to a fault-controlled mosaic carbonate platform with supratidal to subtidal conditions (Moreau et al., 2012). The rapid lateral and vertical facies changes, and the lack of consistent landward or seaward direction also question the existence of a close shoreline (Hamon and Merzeraud, 2008). Bathymetry increased temporally (<~50m) during the Pliensbachian-lower Bajocian interval with the presence of pelagic faunas like Ammonites (Ciszak et al., 1999) and decreased during Bathonian with paleosoil development and intertidal environments well evidenced by theropod footprints (Charcosset et al., 2000; Gand et al., 2018). Deepening resumed during Callovian and Oxfordian (Ciszak et al., 1999).

The upper part of the Jurassic sequence is characterized in the Causses domain and Aquitaine Basin by a karstified erosion surface. In the Aquitaine Basin, this surface is overlain by Upper Cretaceous sediments (Biteau et al., 2006) which are lacking in the small Causses Basin except some Upper Cretaceous sediments found in karst suggesting the presence of a former Cretaceous cover (Bruxelles et al., 1999).

From Early Cretaceous to Late Oligocene, several geodynamical events have affected the south of the Massif Central and the adjacent sedimentary basins. The Aquitaine Basin suffered extension during Early Cretaceous because of the opening of the Bay of Biscay, a lateral extension of the North Atlantic opening (Biteau et al., 2006). During mid-Cretaceous, the South-East basin is characterized by doming – the so-called Durancian event - in the Durance area separating the northern (Vocontian) and the southern (Provence) part of the basin (Masse and Philip, 1976). This emerged land is connected to the French Massif Central, to the west, to the Massif des Maures to the east and is characterized by aerial erosion of Middle Jurassic to Lower Cretaceous rocks and by continental formations like bauxite deposit, trapped in karstic formation in the South-East Basin and the Causses Basin (Combes, 1990). Ongoing deformation

is recognized in the northern part of South-East Basin, as testified by a major angular unconformity at the bottom of the “Senonian” (Coniacian to Maastrichtian) strata (Michard et al., 2010). Several inversion episodes occurred as a consequence of Pyrenean compression which started during Late Cretaceous and reached a climax during Bartonian (Roure et al., 1989). As a consequence, the Aquitaine Basin has gone from an intracontinental to a foreland basin setting (Biteau et al., 2006). In the South-East Basin, marine sedimentation stopped during Late Cretaceous (Schreiber et al., 2011). In the Causses domain, the Pyrenean event induced numerous fault inversions as well as neoformed faults (Blès et al., 1989; Constantin et al., 2004). Oligocene and Miocene are characterized by complex geodynamics combining extension in the South-East Basin (Golfe du Lion opening, Séranne, 1999) and shortening related to Alpine orogeny in the French Alps (Séranne et al., 2002).

Presently, the south of the Massif Central, including the Causses Basin and the Variscan basement, is characterized by high elevation (~1000 m) above neighboring sedimentary basins.

SAMPLING

The sampling strategy adopted for this study involved collecting Lower Jurassic marls for organic matter Rock Eval pyrolysis over a west east transect across the Causses Basin and its western (Aquitaine Basin) and eastern (South-East Basin) boundaries (see sample location - white stars - on Figure 2). Lower Jurassic marl formations (thickness of approximately 100m) are considered as a horizontal layer during deposition on the entire area and its burial might represent a relevant marker. In addition, western (Rouergue), eastern (Cévennes) and northern (Margeride) border evolution of the Causses domain has been characterized using low temperature thermochronology to quantify age and amount of erosion. Sampled areas have been selected where basement rocks suitable for apatite crystal recovery are covered by Lower Jurassic deposits.

METHODS

Rock-Eval Pyrolysis

38 samples of Pliensbachian and Toarcian marls have been collected across the studied area (white stars, Figure 2). Sampling was carried out using a scoop, digging as far as possible in the ground to collect fresh samples containing unoxidized organic matter; samples were then recovered at 25-50 cm below the surface. Sample preparation includes selection of clay ships, drying and crushing. Samples have been analyzed using a RE6 Rock-Eval apparatus at the ISTeP laboratory (Sorbonne Université, France) following the basic/bulk rock method described by Behar et al. (2001), which is a classical analytical procedure devoted to petroleum source rock characterization. Rock-Eval pyrolysis provides numerous parameters (Espitalié et al., 1985; 1986), including (1) hydrogen and oxygen indices (HI and OI) and (2) Tmax, which are both used in the present study . Although the type of organic matter is usually defined by the mean of elemental analysis (Tissot et al., 1971), HI and OI parameters approximate respectively the H/C and O/C atomic ratios which are characterizing the nature of organic matter. Tmax corresponds to the oven temperature at the maximum of hydrocarbon formation peak. Tmax indicates the thermal state of the kerogen from which paleotemperature might be determined (Espitalié et al 1986; Behar et al 2001). Standard deviation of the Tmax is ±2°C. This technique also gives an evaluation of the total organic (TOC) and total inorganic (MinC) carbon content of the rock and only samples with TOC > 0.25 % were used further in this study to determine paleotemperature.

Apatite fission track (AFT) and apatite (U-Th)/He (AHe)

AFT and AHe analyses were performed at the GEOPS laboratory (Université Paris Saclay, France). Classical mineral separation procedures were followed, and grains were picked under a binocular microscope.

Apatite fission-track data were obtained using the external detector method and zeta calibration (Hurford and Green, 1983). Samples were irradiated by thermal neutrons (E<0,25 eV) in the Garching facility of the Technische Universität München (Germany) with a fluence of 5×10^{15} n.cm^{-2}. Etching conditions were 5M HNO_3 for 20 seconds at 20±0.5 °C for apatite crystals and 40% HF for 20 minutes at 20±1 °C for muscovite external detectors. Central ages are calculated using a ζ-value for the dosimeter glass CN5 of 359±8 calibrated by multiple analyses of IUGS apatite age standards (Durango, Fish Canyon, see Hurford, 1990). Only crystals with

sections parallel to the *c*-axis were analyzed. Confined track-lengths have been measured using only TINTs (track-in-track) under a 100x dry objective with a digitizing tablet linked via a drawing tube attached to the microscope. Angle to the *c*-axis was measured for each track length and Dpar values are available to determine the structural/chemical control of apatites on fission-track annealing (Carlson et al., 1999; Barbarand et al., 2003).

AHe ages were measured on carefully selected apatite grains, the dimensions of which were measured along the three axes and placed into a platinum basket. Three to nine replicates were acquired per sample. Ejection factors and sphere equivalent radius have been determined using the Monte Carlo simulation of Gautheron et al. (2012) and alpha ejection stopping distances of Ketcham et al. (2011). Methods for the measurement of the He, U and Th content are similar to those described in Gautheron et al. (2013), U and Th concentrations being measured using a quadrupole ICP-QMS series II CCT Thermo-Electron at LSCE (Gif/Yvette; France). The analysis was calibrated using internal and external age standards, including Limberg Tuff and Durango apatite. Mean AHe ages of 16.6±1.1 Ma and 31.8±0.5 Ma were been measured for the Limberg tuff and Durango yellow apatite respectively, which are in agreement with literature data: 16.8±1.1 Ma for Limberg (Kraml et al., 2006) and 31.4±0.2 Ma for Durango (McDowell et al., 2005). Error on the AHe age at 1 sigma is estimated at 8%, reflecting uncertainty in the ejection factor FT correction and standard dispersion.

Thermal history was determined by QTQt modeling (Gallagher et al., 2009; Gallagher, 2012) that allows inverting AFT and AHe by a Markov chain Monte Carlo sampling method. The inversion code incorporates kinetic models of He diffusion including impact of damage production and annealing proposed by Gautheron et al. (2009), as well as the multi-compositional fission-track annealing model of Ketcham et al. (2007). The modeling proceeds from an initial randomly chosen time-temperature path and set of kinetic parameters, for which a probability that the model fits the data is calculated and the model with the highest probability is retained. This procedure is repeated a large number of times (100,000 iterations have been used here), providing a large number of models with their associated probabilities that allow calculating model statistics.

Thickness of the present-day sedimentary cover

To constrain thermal history modelling, it is necessary to consider the present-day cover over the studied area. A west east transect has been done for the south of the Massif Central to

summarize the present-day remaining sedimentary cover thickness. This transect was built from drill-hole data extracted from the French geological survey (BRGM) database (BSS) considering the Aquitaine and the South-East basin. For the Causses Basin where no drill-hole is available, the sedimentary cover thickness has been evaluated from previous sedimentological studies (Michard and Coumoul, 1978; Ciszak et al., 1999) and from geological map explanatory notes.

RESULTS

Rock-Eval pyrolysis

Total Organic Carbon (TOC) is ranging between 0.26 and 1.78 % for most of the samples and only one sample from the Toarcian "Schistes cartons Formation" level has a TOC of 8.15% (Table 1). Hydrogen index (HI) is ranging for most of the samples between 79 and 305 mgHC/gTOC; the "Schistes cartons" level is characterized by a higher value (666 mgHC/gTOC) (Table 1 and Fig. 3A). Oxygen index (OI) is between 10 and 246 mgCO_2/gTOC, most of the data being lower than 100 mgCO_2/gTOC (Fig. 2). Tmax varies between 430°C and 440°C (Table 1 and Fig. 3B).

OI index shows that, except for some few data, oxidation due to surficial weathering is limited and that organic matter data are meaningful. Following HI and OI relationships (Fig. 3A), the origin of organic matter can be defined as a mixing between marine (Type II) and continental (Type III), except for the "Schistes cartons" level where a marine origin (excellent Type II to Type I) is obvious.

Tmax values are relatively grouped (mean±1σ of 435±3°C) and characterize the beginning of the oil window (Fig. 3B; Tmax of ~430°C, Espitalié et al., 1986). Similar values are observed in the margin of the Aquitaine Basin and of the South-East Basin, in the Causses Basin but also for samples located on the Variscan basement on the present-day borders of these basins (Fig. 2). It appears there is no relationships at all between Tmax values and location or elevation of the samples.

Low temperature thermochronology

Apatite fission-track data are presented for 20 new samples (Table 2, Fig. 4). Most of the data have been acquired on the eastern and northern borders of the Causses Basin and some data are available for the Rouergue border (Fig. 4). Central ages are ranging between 74±5 and 187±6 Ma but most of the data define a narrow range between 101±3 and 133±6 Ma. Four samples on the north of the studied area (Margeride) are systematically older (170±6 and 187±6 Ma) and have shorter mean track length (11.5<MTL<12.1 μm) . All other samples are characterized by MTL > 12.7 μm suggesting a relative rapid cooling. Younger central ages are also measured for most of the samples of the Mont Lozère (74±5 and 98±5 Ma). Dpar values are

homogeneous among samples at ~1.1 µm. All data are characterized by much younger age than crystallization Paleozoic age which testifies from paleotemperatures able high enough to reset of partially reset the FT system.

Apatite (U-Th)/He data have been acquired for seven samples and corrected ages are ranging between 65±5 and 184±15 Ma, sphere equivalent radius between 34 and 135 µm and with eU effective uranium content between 19 and 93 (with two odd values at 146 and 223 ppm) (Table 3, Fig. 4). AHe ages correlated positively with the grain size (i.e. Rs, the sphere equivalent radius; Gautheron and Tassan-Got, 2010) and the eU content for some samples. In addition, one aliquot (MC23E) presents older AHe age and different Th/U ratio than other aliquots from the same sample, that could indicate the presence of undetected thorite of uraninite micrometric inclusions. The age of this aliquot was therefore not used in the following discussion. Five samples (MC20, 23, 26, 31 and 36, representative of samples from the Quercy and the Cévennes areas) are characterized by apatite (U-Th)/He ages younger than FT age. For samples MC38 and MC25, (U-Th)/He ages are respectively similar and older compared to FT ages (Table 3). This may be explained by the sensitivity of AHe which is controlled by temperature but also by the alpha recoil damage dose amount. Thus, dispersed AHe ages reflect protracted thermal history and younger or older AHe ages reflect the combination of different thermal histories and U-Th content (see Ault et al., 2019 for detailed review). Thermal modeling using QTQt integrates all these parameters on He retention (damage production and annealing, and crystal size), and fission track annealing and produces a thermal history that may reproduce both AHe and AFT datasets.

Thermal history has been modeled assuming a large temperature time box for the beginning of the history allowing large freedom of the modeling and surface temperature of 15±5°C is chosen for present. Modeling results are similar among samples and reveal a thermal increase during Jurassic up to temperature around 110±10 °C and cooling starting during Early Cretaceous for sample with AFT ages around 110 and 130 Ma (MC20, 21, 38, Figure 5) and at the end of Early Cretaceous for samples with the younger ages (MC25, 26, 30, 31 and 32, Fig. 5). Samples with the older ages from the Margeride area (MC39, 40, 41 and 42) reveal a temperature increase up to 80±10°C approximately at the same period (see sample MC39, fig. 5). Modeling for all samples is available in the supplementary materials.

DISCUSSION

Thermal history of southern France

Paleotemperature data acquired in this study show that the area, including basement domains and sedimentary basins experienced a similar thermal history during the last 200 Ma.

New low temperature thermochronology data are in agreement with published data on nearby samples (Barbarand et al., 2001; Peyaud et al., 2005, Gautheron et al., 2009; François et al., 2020; Olivetti et al., 2020; Fig. 6). Except for the western border of the South-East Basin, where FT ages are younger, and some FT data in the north of the studied area where ages are older, data are ranging regionally between 80 and 130 Ma. These data show that basement samples underwent a maximum of heating during Late Jurassic and Early Cretaceous. Maximum temperature has been derived from inversion of LTT data and is about 100±10°C. Heating occurred during Late Jurassic and in many cases during Early Cretaceous. Relatively rapid cooling evidenced by MTL > 13 μm occurred at the end of the Early Cretaceous and during Late Cretaceous. Heterogeneity exists among samples which might be due to local variations of paleotemperature or to insufficient statistics. Some samples of the Margeride area share a slightly different thermal history with lower temperature (~80°C) attested by older ages and shorter mean track lengths (sample MC39 on Fig. 5).

Organic matter data are documented for the entire southern sedimentary domain for the first time and data from the Causses domain can be compared with data acquired on the borders of the two large western and eastern French sedimentary basins. On the south of the Causses area, Tmax value for the Toarcian shales are consistent with data measured at 425-430°C by Mailliot et al., (2009) and at 433-440°C measured by Peyaud et al. (2005). On the western Causses Basin, Fonseca et al. (2018) measured equivalent VR of 0.45-0.52% from optical analysis of the organic matter (spore coloration index, algae spectral fluorescence, …). This VR value range is compatible with the beginning of the oil window and in adequacy with our measured Tmax values. Few data have been published on the Aquitaine Basin border but are similar with our results: Qajoun (1994) measured Tmax values of 425-440°C for Lower Jurassic samples from the Quercy; Baudin (1989) measured a value of 434°C and Fonseca et al. (2018) published equivalent VR of 0,42-0,54% for Lower Jurassic samples. Bastianini et al. (2017) found Tmax <430°C for Upper Kimmeridgian limestones. OM data from the western border of the South-East Basin characterize higher Tmax values (430<Tmax<480°C) indicative probably of a thicker sedimentary cover (Disnar, 1994; Pagel et al., 1997).

Specific areas on western and northern borders of the Mont Lozère allow to measure at the same place thermochronological and Tmax data. The two datasets are in agreement and show unambiguously that the basement and the Jurassic sedimentary cover share a common thermal history during Jurassic and likely Cretaceous.

Studies focused on Pb-Zn-Ag ore deposits at the interface between the basement and the South-East and Causses domain in Triassic and/or Lower Jurassic rocks also consider the thermicity from organic matter maturation. Geochemical studies on organic matter of the Trèves ore deposit show that hydrothermal fluids were at the origin of ore formation and dolomitization but also of abnormally high maturity of organic matter (Gauthier et al., 1985; Disnar et Gauthier, 1989; Disnar, 1996): reflectance vitrinite data and Tmax values characterize high temperatures close to the ores (VR>0.7, Tmax>500°C) but data measured in the adjacent limestones are compatible with the beginning of the oil window (VR = 0,4 and Tmax = 430°C). The same observation has been made in the Malines ore deposit where data acquired at distance from the ores are similar to our data (0.45<VR<0.60 and 424<Tmax<441°C) (Disnar, 1996). These hydrothermal fluids have been also characterized by fluid inclusion microthermometry in Les Malines with temperatures ranging from 130°C to 380°C (Ramboz and Charef, 1988). Whatsoever, these hot fluids circulations close to mineralized deposits remain restricted to small areas (Les Malines and Trèves ore deposits) and cannot account for our measured values at the scale of the studied area. Mineralizing fluids are also observed in the western border during Lower Cretaceous (fluorite ores in the Albigeois; Munoz et al., 2005) but again represent local anomalies which cannot be generalized to the entire southern France domain.

The homogeneity of the organic matter data across the entire studied area shows that this domain shares a common thermal history. Considering minimal local variations, the Pliensbachian-Toarcian horizons underwent similar temperatures and define a similar paleodepth across southern Massif Central. This is particularly impressive when considering samples which are located today at contrasting elevations: Jurassic inliers on top of the Mont Lozère granite outcropping today at ~1000m, sedimentary levels at the base of the Causses Basin at ~600m, in the Aquitaine Basin boundary at ~200m and in the center of the Aquitaine and South-East basins at several kilometers.

Origin of the elevated paleotemperatures

High Tmax values for the sedimentary samples may be related to a sedimentary burial as they are not compatible with the present-day thicknesses. Conversion of Tmax into

paleotemperature and depth requires hypotheses on the heat flow evolution and on the thicknesses of the sedimentary cover. Present-day thermal gradient in the Aquitaine Basin has been estimated at 27.1°C/km (Bonté et al., 2010). A 1D thermal modeling on the entire southern Aquitaine Basin has been conducted by Serrano et al. (2006). This modeling assumed a constant heat flow during Mesozoic and Cenozoic and considered maturity of sedimentary rocks and present-day thickness of the sedimentary cover. This modeling concluded that a low mean heat flow of 55 mW/m^2 prevailed in the Aquitaine Basin (Serrano et al., 2006). This value is lower than the present-day value, the gradient value being equivalent to a heat flux of 68 mW/m^2 assuming a mean thermal conductivity of 2.5 W/m/°C. Reconstruction of the present-day sedimentary thicknesses is tedious in the south of the Massif Central as no borehole is available in the Causses domain and significant variations exist at a local scale. Present thicknesses of the Jurassic sedimentary column have been however synthetized from BRGM (french geological survey) geological maps of the area assuming minimum and maximum estimates (Fig. 7). Minimum represents possibly an underestimation as thicknesses are variable at the scale of each geological map and lower amounts of sediment may be deposited at the same place during the entire Jurassic. Similarly, maximum thicknesses may be overestimated. Ciszak et al. (1999) evidenced for example that thicker Middle Jurassic series are observed in the centre of the Causses domain, defined by the authors as the Grands Causses graben; laterally, Middle Jurassic series are reducing in thickness. A cross-section has been drawn across the studied area to visualize the distribution of sedimentary series (Fig. 8). Data for the Aquitaine Basin have been extracted from boreholes and from a west east seismic line (seismic line n°13 in Serrano et al., 2006). Geological maps and data from figure 5 have been used for the central section. Thicknesses along the South-East Basin boundaries are constrained by BRGM borehole data. Figure 6 shows a relative continuity of the Lower and Middle Jurassic series. The same conclusion cannot be stated for the Upper Jurassic series which are largely eroded.

These data available for the reconstruction of the thermal history have been considered using two different approaches: modeling and comparison with other close sedimentary basins. 1D thermal modeling has been therefore carried out using Petromod® software assuming a variable heat flow from 40 to 80 mW/m^2 (maximum corresponding to the Tethys sea opening; see supplementary data for details) and a Jurassic series of ~1000 meters from Toarcian to Tithonian (Portlandian) corresponding to a potential section in the Causses Basin. This thickness represents a raw mean estimate for the Jurassic column deposited in the southern Massif Central from geological maps (Fig. 7). Modeling with an additional ~1000m, which might correspond to Lower Cretaceous sedimentary rocks, produces Tmax data which are in agreement with the measured data in the Pliensbachian-Toarcian series (Fig. 9).

Burial history in accordance with Tmax data can also be estimated by comparing our results to the data available in the Paris Basin. For Tmax values to be compared, we have to assume a similar organic matter composition which is likely to be the case for the upper Lower Jurassic samples, as the late Early Jurassic is a period of uniform deposition of marls accross the European platform (Jenkyns, 1988; Bruneau et al., 2017). Toarcian samples have been studied in the centre of the Paris Basin and displays Tmax values ranging between 420 and 450°C. A similar range of values compared to our data (~430-435°C) is observed at depths between 1800 and 2200 meters (Tissot et al., 1971; Espitalié et al., 1985). Erosion is also determined in the centre of the Paris basin (Demars and Pagel, 1994; Ménétrier et al., 2005) and a few hundred of meters have to be added to these depths (Demars and Pagel, 1994).

Thermal modeling assuming a thermal paleoflux or direct comparison with neighboring basins (Paris Basin) conclude all that a significant sedimentary cover has been deposited and largely eroded. This result is in line with Pagel et al. (1997) extensive work on the western margin of the South-East Basin. These authors unraveled the thermal history by using various organic and inorganic geothermometers (Pagel et al., 1997) and show that paleotemperatures were higher than present-day temperatures. These higher paleotemperatures are explained by erosion of a thick sedimentary pile (1900m) (Pagel et al., 1997).

Assuming our new data and the sedimentary cover estimated by different approaches in the nearby sedimentary realms, we can assume in the southern Massif Central an erosion of ~1000m in the Causses domain and on the Aquitaine border and ~2000m for the Variscan basement.

Other causes that affected the maximum paleotemperatures than burial may be also considered but their real impact is difficult to evaluate. Increase of the heat flow may be related to deep processes. No evidence of magmatic input during Mesozoic is however observed except the very local (small volume) Les Vignes submarine Bathonian basaltic lavas (Bellon et al., 1986). Other volcanic rocks witnessing an increase of the heat flux are largely distributed in the southern Massif Central but correspond to Miocene to Pliocene activity (Dautria et al., 2010) which have not been recorded by organic matter and low temperature thermochronology data. Large mantle anomalies are recorded southward in front of the present-day Pyrenees orogen (Clerc et al., 2012) but appear to be confined to this domain.

To conclude, this study suggests that a significant (> 1 to 2 km thick depending on the area) sedimentary cover deposited in present-day sedimentary realm (Causses domain, South-East and Aquitaine basins boundaries) but also over the present-day Massif Central basement. Although low bathymetry facies in the Jurassic series of the Causses domain led some authors to suggest the proximity of a shoreline (see geological context above), implying an emerged area at

that time, our data discard this facies-based interpretation. The whole studied area did subside during the Jurassic and Early Cretaceous time and the continuous infill or subsidence slowing of this vast basin may explain the low bathymetry recorded in some of the formations. Figure 10 proposes a new light on the paleogeography of the southern Massif Central with the definition of a large marine realm during Jurassic times.

Origin of the Lower Cretaceous erosion event

Low temperature thermochronology suggests a cooling/erosion event starting during late Lower Cretaceous. Organic matter data plead for the hypothesis of an overburial to explain high paleotemperatures. The deposition of this Jurassic and possibly Lower Cretaceous sedimentary cover and its erosion during late Early Cretaceous is here discussed in the light of the regional geological history.

The two large sedimentary basins of southern France, Aquitaine Basin and South-East Basin, share a common history during parts of the Mesozoic but have been considered separately as they are now separated by the southern Massif Central. The sedimentation is homogeneous during Upper Triassic, when Aquitaine and South-East basins are isolated and characterized by the deposit of an important evaporitic sequence. In the Causses Basin, Triassic rocks are present in the southern part of the basin and remain continental except in the east where evaporitic deposit can be observed. This suggests that the Causses Basin remained a continental realm during Upper Triassic and was not connected to the neighboring basins. Marine environments are observed from Hettangian with the development of a passive continental margin of the Tethys Ocean corresponding to the South-East basin. Fault controlled subsidence occurred during Lower and Middle Jurassic times and from Late Jurassic a general thermal subsidence is recorded with the deposition of thick uniform sedimentary series (Bonijoly et al., 1996). In the Aquitaine Basin, the opening of the Atlantic Ocean was contemporaneous during Jurassic with the development of a carbonate platform extending over the entire basin (Biteau et al., 2008). During this period, the Causses Basin is connected to the Aquitaine Basin by the Rodez Strait and to the South-East Basin by the Cévennes High. Remnants of a lower Jurassic sedimentary cover are recognized in different parts of the basement of southern Massif Central, demonstrating that the present-day geometry (border vs basin) was

not acquired at that time although thicknesses are generally reduced on the Cévennes border (Charcosset, 2000).

Although a thick Lower Cretaceous series is recorded in the South-East Basin, a regional unconformity characterizes the transition between the Jurassic and the Cretaceous in the Aquitaine Basin. An extensive karstification correlated to this unconformity in the underlying Jurassic sedimentary rocks is observed in the eastern border of the Aquitaine Basin (Simon-Coinçon et al., 1997). Level of erosion is variable in the different portions of the basin: Upper Jurassic in the Causses domain, mainly Lower Jurassic in the Rodez Strait, Middle Jurassic in the Cévennes High. This erosion might have removed the entire sedimentary section as it happens on the Cévennes and Rouergue basements; only methods such as those deployed here might be able to envisage this sedimentary cover that we estimate to have been more than 2 km thick.

This unconformity and related erosion evidenced and quantified in this work might be linked to a mid-Cretaceous event that has been recognized and well characterized by the presence of bauxites in the south of France (Combes, 1990). Allochthonous bauxites are distributed along a surface that is sealed by middle Cenomanian deposits. Surrounding rocks are of various ages (Lower Jurassic to Early Cretaceous) depending of the morphology of the erosion surface. This bauxitic event has been interpreted related to a large geodynamical reorganization in the South-East Basin with the development of a positive structure, the "Durancian isthmus" separating the subsiding Vocontian and Provençal basins (Masse and Philip, 1976; Guyonnet-Benaize et al., 2010). The origin of this structure is not well established but seems to have occurred when the Iberian block drifted eastward. This motion of the Iberian block is associated with the opening of the Bay of Biscay in the Atlantic domain and the beginning of the Pyrenean basin closure. Extension in the Bay of Biscay occurred in the Late Jurassic to Early Cretaceous in relationship to the northward propagation of the Atlantic rift. Extreme crustal thinning in the Bay of Biscay resulted in continental breakup and seafloor spreading initiation during latest Aptian to early Albian (~115-110 Ma) time (Montadert et al., 1979). This extension arose also by exhumation of the north Pyrenean zone in the southern Aquitaine Basin (Lagabrielle et al., 2010; Clerc et al., 2012). Timing of this exhumation might be approached by its associated metamorphism, volcanism and hydrothermalism between 115 and 85 Ma (Boulvais 2016). These events traduced a major contemporary geodynamical reorganization which has affected a very large surface as evidenced by our thermochronological data.

CONCLUSION

For a long time, the evolution of the south of the Massif Central domain, including the Causses domain and the Variscan basement, has been debated considered either as a continental realm during most Mesozoic and Cenozoic times because of its present-day elevation (around 1000 m above the neighboring basins) and the absence of sedimentary witnesses or as an area of marine sedimentation. Burial of sedimentary and magmatic rocks has been studied using data from organic matter evolution and low temperature thermochronology to test these hypotheses.

The organic matter data on Lower Jurassic marls in the Causses Basin and the borders of the Aquitaine and South-East basins (430°C≤Tmax≤440°C) correspond to the beginning of the oil window. Apatite fission-track data on the Rouergue and Cévennes basements (ages ranging between 74±5 and 187±6 Ma and MTL between 11.5±0.3 and 13.6±0.1 μm) and (U-Th)/He on apatite data (ages ranging between 65±5 and 184±15 Ma) and their thermal modelling indicate that apatite crystals were buried at temperature around 100±10°C at the end of Jurassic or beginning of Early Cretaceous. The onset of cooling below these temperatures is between 150 and 100 Ma.

These data are interpreted to be related to the deposition of 1000 to 2000 m of sediment during Jurassic and probably Early Cretaceous in a large portion of the south of France from the Aquitaine Basin to the South-East Basin across the Causses domain and in particular on top of the Rouergue and Cévennes basements.

This sedimentary section has been eroded during a main episode of erosion at the end of Early Cretaceous (mid-Cretaceous), and in all cases before the beginning of Late Cretaceous. The origin of this episode might be related to large changes in the paleogeography of southern France and reorganization of the framework between Iberia and Europe, including opening of the Biscay bay, inversion on the Pyrenean margin and formation of the Durancian isthmus. This Lower Cretaceous period appears as a key period for the geological evolution of southern France.

These results testify of a connection between the Aquitaine Basin, the south Massif Central and the South-East Basin during Jurassic and probably Early Cretaceous. The present-day geometry, implying a kilometer scale surface uplift, has been further acquired later.

Acknowledgements

The authors thank Schlumberger for the Petromod® licence, IRSN for the support of the P. Préhaud M2 internship and of the field work and Andrew Carter (Department of Earth and Planetary Sciences, Birkbeck College, London) for some unpublished fission-track data. Louise Bordier is thanked for her help during the U and Th measurement and Eric Douville for access to the ICP-QMS.

References

Alabouvette B., Azéma C., Bodeur Y., Debrand-Passard S., 1984, Le Crétacé supérieur des Causses, *Géologie de la France* 1-2, 67-73.

Ault, A. K., Gautheron, C., and King, G. E., 2019, Innovations in (U-Th)/He, fission-track, and trapped-charge thermochronometry with applications to earthquakes, weathering, surface-mantle connections, and the growth and decay of mountains: *Tectonics*, v. 38.

Barbarand J., Lucazeau F., Pagel M., Séranne M., 2001, Burial and exhumation history of the South-Eastern Massif Central (France) constrained by apatite fission track, *Tectonophysics* 335, 275-290.

Barbarand J., Carter A., Wood I., Hurford T., 2003, Compositional and structural control of fission-track annealing in apatite, *Chemical Geology 198*, 107-137.

Bastianini L., Caline B., Hoareau G., Bonnet C., Martinez M., Lézin C., Baudin F., Brasier A., Guy L., 2017, Sedimentary characterization of the carbonate source rock of Upper Kimmeridgian Parnac Formation of the Aquitaine Basin (Quercy area), *Bulletin de la Société Géologique de France* 188 (5): 32. https://doi.org/10.1051/bsgf/2017197

Baudin F., 1989, Caractérisation géochimique et sédimentologique de la matière organique du Toarcien téthysien (Méditerranée, Moyen-orient). Significations paléogéographiques, Thèse de l'Université P. et M. Curie. Mémoire des Sciences de la Terre, 89-30, 350 p.

Baudrimont, A.F. and Dubois, P., 1977, Un Bassin Mésogéen du domaine péri-alpin: Le Sud-Est de la France. *Bull. Cent. Rech. Explo-Prod. Elf*. 1, 261–308.

Behar F., Beaumont V., De B. Penteado H.L., 2001, Rock-Eval 6 Technology: Performances and Developments, *Oil & Gas Sciences and Technology- Rev*. IFP 56, 2, 111-134.

Bellon H., Fabre A., Sichler B., Bonhomme M.G., 1986, Contribution to the numerical calibration of the Bajocian-Bathonian boundary: ^{40}K-^{40}Ar and paleomagnetic data from les Vignes basaltic complex (Massif Central, France), *Chemical Geology (Isotope Geoscience Section)* 59, 155-161.

Biteau J.J., Le Marrec A., Le Vot M., Masset J.M., 2006, The Aquitaine basin, *Petroleum Geosciences* 12, 247-273.

Blès J.L., Bonijoly D., Castaing C., Gros Y., 1989, Successive post-variscan stress fields in the French Massif Central and its borders (Western European plate): comparison with geodynamic data, T*ectonophysics* 169, 79-111.

Boiron M.-C., Cathelineau M., Richard A., 2010, Fluid flows and metal deposition near basement /cover unconformity: lessons and analogies from Pb–Zn–F–Ba systems for the understanding of Proterozoic U deposits, Geofluids 10, 270-292.

Bonijoly D., Perrin J., Roure F., Bergerat F., Courel L., Elmi S., Mignot A., and the GPF team, 1996, The Ardèche palaeomargin of the South-East Basin of France: Mesozoic evolution of a part of the Tethyan continental margin (Géologie Profonde de la France programme), Marine and Petroleum Geology 13, 6, 607-623.

Bonté D., Guillou-Frottier L., Garibaldi C., Bourgine B., Lopez S., Bouchot V., Lucazeau F., 2010, Subsurface temperature maps in French sedimentary basins: new data compilation and interpolation, *Bull. Soc. Géol. Fr.* 181, 4, 377-390.

Boulvais Ph., 2016, Fluid generation in the Boucheville Basin as a consequence of the North Pyrenean metamorphism, *C.R. Géosciences* 348, 301-311.

Bruneau B., Chauveau B., Baudin F., Moretti I., 2017, 3D stratigraphic forward numerical modelling approach for prediction of organic-rich deposits and their heterogeneities, *Marine and Petroleum Geology* 82,1-20, 10.1016/j.marpetgeo.2017.01.018.

Bruxelles P., Ambert P., Guendon J.L., Tronchetti G., 1999, Les affleurements de Crétacé supérieur sur les Grands Causses méridionaux (France), *C.R. Acad. Sciences Paris 329*, 705-712.

Carlson W.D., Donelick R.A., Ketcham R.A., 1999, Variability of apatite fission-track annealing kinetics: I. Experimental results, *American Mineralogist, 84*, 1213-1223.

Charcosset P., 2000, Synthèse paléogéographique et dynamique du bassin caussenard (Sud de la France) au cours du Bathonien (Jurassique moyen), *Eclogae geol. Helv.* 93, 53-64.

Charcosset P., Combes P.J., Peybernès B., Ciszak R., Lopez M., 2000, Pedogenic and karstic features at the boundaries of Bathonian depositional sequences in the Grands Causses area (southern France): stratigraphic implications, *Journal of Sedimentary Research* 70, 1, 255–264.

Ciszak R., Peybernès B., Thierry J., Fauré Ph., 1999, Synthèse en termes de stratigraphie séquentielle du Dogger et de la base du Malm dans les Grands Causses, *Géologie de la France* 4, 45-58.

Clerc C., Lagabrielle Y., Neumaier M., Reynaud J.Y., De Saint Blanquat M., 2012, Exhumation of subcontinental mantle rocks: evidence from ultramafic-bearing clastic deposits nearby the Lherz peridotite body, French Pyrenees, *Bull. Soc. Geol. France* 183, n°5, 443-459.

Combes P.-J., 1990, Typologie, cadre géodynamique et genèse des bauxites françaises, *Geodinamica Acta* 4, 2, 91-109.

Constantin J., Peyaud J.B., Vergély P., Pagel M., Cabrera J., 2004, Evolution of the structural fault permeability in argillaceaous rocks in a polyphased tectonic context, *Physics and chemistry of the earth 29*, 25-41.

Curnelle R., Dubois P., 1986, Evolution Mésozoïque des grands bassins sédimentaires français : bassin de Paris, d'Aquitaine et du Sud-Est, *Bull. Soc. Geol. France (8)*, t. II, n°4, 529-546.

Dautria J.M., Liotard J.-M., Bosch D., Alard O., 2010, 160 Ma of sporadic basaltic activity on the Languedoc volcanic line (Southern France): A peculiar case of lithosphere–asthenosphere interplay, L*ithos* 120, 202-222.

Demars C., Pagel M., 1994, Paléotempératures et paléosalinités dans les grès du Keuper du basin de Paris: inclusions fluids dans les minéraux authigènes, *C.R. Acad. Sciences Paris* 319, 427-434.

Disnar J.R., 1994, Determination of maximum paleotemperatures of burial (MPTB) of sedimentary rocks from pyrolysis data on the associated organic matter: basic principles and practical application, *Chemical Geology* 118, 289-299.

Disnar J.R., 1996, a comparison of mineralization histories for two MVT deposits, Trèves and Les Malines (Causses basin, France), based on the geochemistry of associated organic matter, *Ore Geology Reviews 11*, 133-156.

Disnar J.R., Gauthier B. (1989) Contribution of organic geochemistry to regional exploration and characterization of Mississippi Valley-type mineralization in the Causses basin (France), *Journal of Geochemical Exploration* 32, 401-403.

Dubois P., 1985, Notes karstologiques sur les Grands Causses, *Bull. Soc. Lang. Géog 19 (3-4)*, 197-226.

Einsele G., 2000, Sedimentary Basins, Springer, 727p.

Espitalié J., Deroo G., Marquis F., 1985 La pyrolyse Rock-Eval et ses applications, deuxième partie, *Rev. Inst. Fr. Pétrole* 40 (6), 754-784.

Espitalié J., Deroo G., Marquis F., 1986, La pyrolyse Rock-Eval et ses applications, troisième partie, *Rev. Inst. Fr. Pétrole* 41 (1), 73-89.

Faure M., Lardeaux J.M., Ledru P., 2009, A review of the pre-Permian geology of the Variscan French Massif Central, *C.R. Geosciences* 341, 202-213.

Fonseca C., Mendonça J.O., Mendonça Filho J.G., Lézin C., Duarte L.V., 2018, Thermal maturity assessment study of the late Pliensbachian-early Toarcian organic-rich sediments in southern

France: Grands Causses, Quercy and Pyrenean basins, *Marine and Petroleum Geology* 91, 338-349.

François T., Barbarand J., Wyns R. (2020) Lower Cretaceous inversion of the European Variscan basement: record from the Vendée and Limousin (France). International Journal of Earth Sciences https://doi.org/10.1007/s00531-020-01875-z.

Galbraith, R.F., Laslett, G. M., 1993, Statistical models for mixed fission-track ages, *Nucl. Tracks Radiat. Meas*., 21, 459-470.

Gallagher K., Charvin K., Nielsen S., Sambridge M., Stephenson J., 2009, Markov chain Monte Carlo (MCMC) sampling methods to determine optimal models, model resolution and model choice for Earth Science problems, *Mar. Pet. Geol.*, **26**, 525–535.

Gallagher K., 2012, Transdimensional inverse thermal history modelling for quantitative thermochronology, *JGR, 117 (B02408)*, 16.

Gand G, Fara E., Durlet C., Moreau J.-D., Caravaca G., Baret L., André D., Lefillatre R., Passet A., Wiénin M., Gély J.P., 2018, Archosaurian trackways: itKayentapus ubacensis nov. isp. (theropods) and crocodylomorphs from the Bathonian of the Grands-Causses (France). Palaeo-biological, environmental and geographical implication, *Annales de Paléontologie* 104, 183-216.

Gautheron, C. and Tassan-Got, L. 2010. A Monte Carlo approach of diffusion applied to noble gas/helium thermochronology. *Chem. Geol.* 273, 212-224.

Gautheron C., Tassan-Got L., Barbarand J., Pagel M., 2009, Effect of alpha-damage annealing on apatite (U-Th)/He thermochronology, *Chem. Geol., 266*, 166-179.

Gautheron C., Tassan-Got L., Ketcham R.A., Dobson K.J., 2012, Accounting for long alpha-particle stopping distances in (U-Th-Sm)/He geochronology: 3D modelling of diffusion, zoning, implantation and abrasion, *Geochim. Cosmochim. Acta, 96*, 44-56.

Gautheron, C., Barbarand, J., Ketcham, R., Tassan-Got, L., van der Beek, P. A., Pagel, M., Pinna-Jamme, R., Couffignal, F., and Fialin, M., 2013, Chemical influence on α-recoil damage annealing in apatite: implications for (U-Th)/He dating: *Chem. Geol*., 351, p. 257-267.

Gauthier B., Disnar J.-R., Macquar J.-C, Trichet J. (1985) Pétrographie de la matière organique des series carbonates liasiques du gîte Zn-Pb de Trèves (Gard, France). Implications génétiques, *C.R. Acad. Sciences 300* (II), 9, 413-416.

Guyonnet-Benaize C., Lamarche J., Masse J-P., Villeneuve M., Viseur S., 2010, 3D structural modelling of small-deformations in poly-phase faults pattern. Application to the Mid-Cretaceous Durance uplift, Provence (SE France), *Journal of Geodynamics 50*, 81-93.

Hamon Y., Merzeraud G., 2008, Facies architecture and cyclicity in a mosaic carbonate platform: effects of fault-block tectonics (Lower Lias, Causses platform, south-east France), *Sedimentology* 55, 155–178.

Hurford A.J., 1990, Standardization of fission track dating calibration: Recommendation by the Fission Track Working Group of the I.U.G.S. Subcommission on Geochronology, *Chemical Geology: Isotope Geoscience section 80*, 171-178.

Hurford A.J., Green P.F., 1983, The zeta age calibration of fission-track dating, *Chemical Geology: Isotope Geoscience section* 1, 285-137.

Jenkyns H.C. (1988) The early Toarcian (Jurassic) Oceanic Anoxic Event: stratigraphic, sedimentary and geochemical evidence, *American Journal of Science* 288, 2, 101-151.

Ketcham R.A., Carter A., Donelick R.A., Barbarand J., Hurford A.J., 2007, Improved modelling of fission-track annealing in apatite, *American Mineralogist 92*, 5-6, 799-810.

Ketcham R.A., Gautheron C., Tassan-Got L., 2011, Accounting for long alpha-particle stopping distances in (U-Th-Sm)/He geochronology: refinement of the baseline case, *Geochim. Cosmochim. Acta, 75*, 7779-7791.

Kraml M., et al., 2006, A new multi-mineral age reference material for $^{40}Ar/^{39}Ar$, (U-Th)/He and fission track dating methods: The Limberg t3 tuff. *Geostandards and Geoanalytical Research, 30*, 73-86.

Lagabrielle Y., Labaume P., De Saint Blanquat M., 2010, Mantle exhumation, crustal denudation and gravity tectonics during Cretaceous rifting in the Pyrenean realm (SW Europe): Insights from the geological setting of the lherzolite bodies, *Tectonics* .29, TC4012, doi :10.1029/2009TC002588.

Mailliot, S., Mattioli, E., Bartolini, A., Baudin, F., Pittet, B., Guex, J., 2009, Late Pliensbachian-Early Toarcian (Early Jurassic) environmental changes in an epicontinental basin of NW Europe (Causses area, central France): a micropaleontological and geochemical approach, *Palaeogeogr. Palaeoclimatol. Palaeoecol*. 273, 346–364. https://doi.org/10.1016/j.palaeo.2008.05.014.

Masse, J.-P., Philip, J., 1976. Paléogéographie et tectonique du Crétacé moyen en Provence : révision du concept d'isthme durancien. *Revue de Géographie physique et de Géologie dynamique* 18 (1), 49–66.

McDowell F.W., McIntosh W.C., Farley K.A., 2005, A precise ^{40}Ar-^{39}Ar reference age for the Durango apatite (U-Th)/He and fission-track dating standard, *Chem. Geol., 214*, 249-263.

Ménétrier C., Elie M., Martinez L., Le Solleuz A., Disnar J.-R., Robin C., Guillocheau F., Rigollet C. (2005) Estimation de la température maximale d'enfouissement du Toarcien et du Callovo-Oxfordien au centre du bassin de Paris par les marqueurs organiques, *C. R. Geoscience* 337 1323–1330.

Michard, A. G., Coumoul, A. (1978). La sédimentation liasique dans les Causses : contrôle des minéralisations Zn-Pb associées au Lotharingien. *Bull BRGM*., sect II., 2, 57-120.

Michard A., Dumont T., Andreani L., Loget N., 2010, Cretaceous folding in the Devoluy mountains (Subalpine chains, France): gravity-driven detachment at the European paleomargin versus compressional event, *Bull. Soc. Geol. Fr.*, t 181, n°6, 565-581.

Montadert L., Roberts D. G., De Charpal O., Guennoc P., 1979, Rifting and subsidence of the northern continental margin of the Bay of Biscay, in Initial Reports of the Deep Sea Drilling Project, vol. 48, edited by L. Montadert et al., pp. 1025–1060, US Government Printing Office, Washington, D. C.

Moreau J.-D., Gand G., Fara E., Michelin A., 2012, Biometric and morphometric approaches on Lower Hettangian dinosaur footprints from the Rodez Strait (Aveyron, France), *C. R. Palevol* 11, 231-239.

Munoz M., Premo W.R., Courjault-Radé P., 2005, Sm–Nd dating of fluorite from the worldclass Montroc fluorite deposit, southern Massif Central, France, *Mineralium Deposita* 39: 970–975.

Pagel M., Braun J-J., Disnard J.R., Martinez L., Renac C., Vasseur G., 1997, Thermal history constraints from studies of organic matter, clay minerals, fluid inclusions and apatite fission tracks at the Ardèche paleo-margin (BA1 drill hole, GPF Program), France, *Journal of Sedimentary Research* 67, 1, 235-245.

Peyaud J.B., Barbarand J., Carter A., Pagel M., 2005, Mid Cretaceous uplift and erosion on the Northern margin of the ligurian Tethys deduced from thermal history reconstruction, *Int. J. Earth Sci. 94*, 462-474.

Qajoun, A., 1994, Le Toarcien du Quercy Septentrional : stratigraphie et micropaléontologie. Strata 2 (22), 236. Available on https://strata.fr/pdf/strata1994-2.22-quajoun-quercy.pdf.

Olivetti, V., Balestrieri, M., Godard, V., Bellier, O., Gautheron, C., Valla, P., Zattin, M., Faccenna, C., Pinna-Jamme, R. and Manchuel, K., 2020. Cretaceous and late Cenozoic uplift of the eastern French Massif Central: insights from low-temperature thermochronometry. *Lithosphere* 12, 133-149.

Ramboz C., Charef A. (1988) Temperature, pressure, burial history, and Paleohydrology of the Les Malines Pb-Zn Deposit: reconstruction from aqueous inclusions in barite, *Economic Geology* 83,784-800.

Romans B.W., Castelltort S., Covault J.A., Fildani A., Walsh J.P., 2016, Environmental signal propagation in sedimentary systems across timescales, *Earth-Science Reviews* 153, 7-29.

Roure, F., P. Choukroune, X. Beràstegui, J. A. Muñoz, A. Villien, P. Matheron, M. Bareyt, M. Séguret, P. Camara, and J. Déramond (1989) ECORS deep seismic data and balanced cross sections: Geometric constraints on the evolution of the Pyrenees, *Tectonics* 8, 1, 41–50, doi:10.1029/TC008i001p00041

Schreiber D., Giannerini G., Lardeaux J.M., 2011, The Southeast France basin during Late Cretaceous times: The spatiotemporal link between Pyrenean collision and Alpine subduction. *Geodinamica Acta* 24, 1, 21-35.

Séranne M. (1999) The Gulf of Lion continental margin (NW Mediterranean) revisited by IBS : An overview. In : Durand, B., Jolivet, L., Horvatn, E & Séranne, M. (eds) The Mediterranean Basins : Tertiary Extension within the Alpine Orogen. Geological Society, London, Special Publications, 156, 15-36.

Séranne M., Camus H., Lucazeau F., Barbarand J., Quinit Y., 2001, Surrection et érosion polyphasée de la bordure cévénole. Un exemple de morphogénèse lente, *Bulletin de la Société Géologique de France 173, 2, 97-112*.

Serrano O., Delmas J. Hanot F., Vially R., Herbin J.-P., Houel P., Tourlière B., 2006, Le bassin d'Aquitaine : valorisation des données sismiques, cartographie structurale et potentiel pétrolier, Ed. BRGM, 245p, 142 figures, 17 tables, 17 annexes.

Simon-Coinçon R., Thiry M., Schmitt J.-M. (1997) Variety and relationship of weathering features along the early Tertiary paleosurface in the southwestern French Massif Central and the nearby Aquitaine Basin, *Palaeogeography, Palaeoclimatology, Palaeoecology* 129, 51-79.

Tissot B., Califet-Debyser Y., Deroo G., Oudin J.L., 1971, Origin and evolution of hydrocarbons in Early Toarcian Shales, Paris Basin, France, *American Association of Petroleum Geologist Bulletin* 55, 2177-2193.

TABLES

Table 1: Rock-Eval pyrolysis results. S2 (in mg/g of rock) the quantity of thermally generated cracked hydrocarbons ; HI, the Hydrogen Index (in mg/g of rock), OI, the Oxygen Index (in mg CO2/g TOC), and Tmax, the temperature at which the largest quantity of hydrocarbons is released upon cracking.

Table 2: Sample details and results including sampling locality, lithology, WGS84 projection system coordinates and elevation.

n - number of apatite crystals counted; s, i and d subscripts denote spontaneous, induced and dosimeter; ρ – track density (x105 tracks/cm2); N - number of tracks counted; P(χ2) - probability of obtaining Chi-square value (χ2) for n degrees of freedom (where n = number of crystals - 1); Age ± 1σ - central age ± 1 standard error (Galbraith and Laslett, 1993); MTL - mean track length (μm); SD - standard deviation of track length distribution (μm); N(L) - number of horizontal confined tracks measured ; Dpar - average etch pit diameter parallel to c. Ages were calculated using the zeta calibration method (Hurford and Green, 1983), glass dosimeters CN-5, and a zeta value of 359± 8 (JB).

Table 3: (U-Th)/He results

Rs is the sphere equivalent radius
* dates are corrected from alpha ejection factor (Ketcham et al., 2011; Gautheron et al., 2012).

FIGURES

Figure 1: A. Geographical sketch and topography of the studied area; B. Geological map of the studied area across the eastern border of the Aquitaine Basin and the western border of the South-East basin through the southern Massif Central and the small Causses Basin. The dotted line represents the cross section shown in figure 8. Stars (SBD, SML, SAC and VAN) correspond to boreholes used in the cross-section. The Treves and Les Malines deposits are localized on the SW and S Cevennes respectively by a t and a m in the center of hexagons.

Figure 2: Sample distribution. Stars represent the sites which have been sampled for organic matter study. Numbers close to the stars are the Tmax values in °C. Black circles correspond to the sites studied for low temperature thermochronology; codes for samples are presented. White circles are sampling sites for apatite fission-track data from literature (Barbarand et al., 2001; Peyaud et al., 2005; François et al., in review).

Figure 3: Organic matter results. A: HI *versus* OI diagram; B: HI *versus* Tmax diagram (after Espitalié et al., 1985; 1986). Standard deviation for OI and HI is 10 mg HC/g TOC; standard deviation on Tmax measurement is 2°C.

Figure 4: distribution of the low-temperature thermochronology data. Fission track results correspond to mean age and mean length; He ages (in blue) are individual corrected ages.

Figure 5: Thermal modeling for representative samples studied by low temperature thermochronology. Sample MC39 characterizes the evolution of the Margeride area where ages are higher than in other domains of the study. Sample MC20 is representative of the thermal history of the Quercy domain. Samples MC38 and MC30 characterize the different rates of exhumation of the Cévennes area. Modeling for all samples is proposed in the supplementary data. For each modeling, text in regular correspond to the measured data, in bold to the modeled data.

Figure 6: Presentation of the fission track data available for the south Massif Central area including data from literature (Barbarand et al., 2001; Peyaud et al., 2005; François et al., 2020) and data from this study.

Figure 7: Subsidence curves are presented for the different areas assuming minimum and maximum estimates. Data correspond to the present-day thicknesses of the Jurassic sedimentary cover recorded by the different geological maps of the studied area Names correspond to geological maps defined for the different sectors. Dotted lines represent the Aquitaine Basin margin. Rodez strait is defined only by the geological map of Rodez. Sabadel corresponds to a borehole, located in the Quercy, crossing the Mesozoic and Paleozoic series; its location is presented in figure 7.

Figure 8: West-East transect across the South of the Massif Central. The Sillon Houiller expressed in its southern part by the Villefranche Fault and the Cévennes Fault are drawn. Data from the following boreholes have been gathered from the French geological survey (brgm)

database (BSS). SML: Saint Martin Labouval; SBD: Sabadel; CPG: Campagnac; SLL: Sauveterre La Lémance; CC:Clairac; CB: Caubon on the Aquitaine Basin side. SAC: Saint André de Cruzières and VAN: Vallon Pont d'Arc on the South-East Basin. No deep borehole exists in the Causse Basin and the Rodez Strait; geological maps from the brgm have been used to define the sedimentary thickness. Name of the geological maps is listed on top of the cross-section.

Figure 9: 1D thermal modeling of a section observed in the southern Causses Basin (Pas de l'Escalette). Present-day sedimentary succession ranges from Triassic to Tithonian with a thickness of ~1600m; thickness above Pliensbachian marls is about 1000m. Tmax values comparable to measured values (grey box) in this study are not compatible with this preserved section. An additional 1000m of Lower Cretaceous series has been considered in this modeling to match model and data. Modeling hypotheses are presented in the supplementary data including paleobathymetry between 0 and 150m, mean surface temperature between 20 and 30°C and heat flow between 40 and 80 mW/m^2. Heat flow value starts at 48 mW/m^2, increases during Tethys ocean opening to 80mW/m^2 and cools down to 40 mW/m^2.

Figure 10: Paleogeographic reconstruction of the south of the Massif Central during (a) Early Lias, (b) Middle and Late Jurassic and (c) Early Cretaceous (modified after Curnelle and Dubois, 1986, Biteau et al., 2006 and the BRGM underground database)

Table 1

Number	Locality	Latitude	Longitude	Host formation	S2 (mg/g)	Tmax (°C)	TOC wt%	HI (mg HC/g TOC)	OI (mg CO2/g TOC)	MinC (%)
1	Rosières	44.46	4.24	Dom/Toarcian	0.33	439	0.4	82	45	5.09
2	Les Alvelas 1	44.36	4.17	Toarcian	0.53	440	0.45	118	36	4.45
3	Montbel1	44.55	3.69	Toarcian	1.05	439	0.84	125	27	3.7
4	Montbel 2	44.55	3.69	Toarcian	1.1	438	0.84	131	26	2.81
5	Saint Bauzille	44.478	3.512	Domerian	1.06	435	0.82	129	28	1.84
6	Les Bondons	44.398	3.593	Toarcian	0.97	436	0.84	115	44	2.51
7	Ispagnac	44.382	3.525	Toarcian	0.63	431	0.64	98	89	3.84
8	Perjuret 1	44.208	3.514	Toarcian	0.91	434	0.59	154	69	4.38
9	Perjuret 2	44.21	3.52	Toarcian	0.94	431	0.91	101	66	3.61
10	Perjuret 3	44.2	3.51	Toarcian	0.99	434	0.85	116	26	6.59
11	Salvinsac	44.2	3.453	Toarcian	1.27	431	0.75	169	39	4
12	Lugagnac	44.19	3.11	Domerian	1.05	438	0.9	117	64	1.85
13	Montjardin haut	44.13	3.4	Toarcian	1.25	433	1.02	123	53	2.87
14	Montjardin bas	44.13	3.4	Toarcian	1.62	432	1.07	151	23	2.43
15	D277-1	43.98	3.16	Toarcian	2.32	438				
16	Tournemire tunnel	43.97	3.01	Toarcian	3.99	434	1.31	305	13	1.76
17	D277-2	43.96	3.04	Late Toarcian	3.18	438	1.53	208	18	1.41
18	D23	43.96	3.04	Toarcian	1.32	436	1.09	107	38	1.17
19	St-Jean-D'Alcapiès	43.95	3	Dom/Toarcian	0.25	437	0.26	96	246	1.41
20	Cornus	43.9	3.18	Early Toarcian	0.72	435	0.67	107	79	2.29
21	St Xist	43.84	3.14	Early Toarcian	0.6	432	0.64	94	36	3.12
22	Le Clapier	43.83	3.168	Dom/Toarcian	0.44	434	0.56	79	66	3.43
23	Les Sièges	43.82	3.25	Late Toarcian	1.95	435	1.18	165	53	1.9
24	Madières	43.85	3.28	Late Toarcian	1.66	436	1.04	160	30	3.22
25	Muret-le-Château	44.49	2.57	Dom/Toarcian	2.17	436	1.17	185	23	1.9
26	Alséroque	44.46	2.48	Toarcian	3.19	438	1.26	253	17	1.2
27	Les Brunhes	44.44	2.68	Toarcian	0.52	437	0.61	85	69	0.39
28	Ayrinhac	44.38	2.8	Toarcian	1.41	432	0.92	153	38	3.59
29	Agen	44.35	2.67	Toarcian	0.29	434	0.28	104	200	0.65
30	Sévérac-Le-Château	44.32	3.07	Early Toarcian	54.26	432	8.15	666	10	4.89
31	Malpeyre	44.55	2.07	Toarcian	3.18	431	1.56	204	28	1.48
32	St Rémy	44.4	2.03	Toarcian	1.75	430	1.03	170	208	0.79
33	La Farette	44.33	1.92	lower Jurassic	0.78	434	0.74	105	99	3.11
34	Pech Laumet 2	44.33	1.86	Toarcian	3.35	438	1.48	226	16	1.08
35	Pech Laumet 1	44.28	1.85	Toarcian	0.38	439	0.4	95	178	0.63
36	St-Antonin	44.16	1.77	Toarcian	1.55	437	1	155	161	1.67
37	Penne	44.08	1.74	Toarcian	0.52	435	0.51	102	45	6.1
38	Bruniquel	44.05	1.67	Toarcian	3.77	434	1.78	212	27	0.7

Table 2

Code	*Name*	*Lithology*	*Long E*	*Lat N*	*Elev.* (m)	n	ρ_s	N_s	ρ_i	Ni	ρ_d	N_d	P(χ^2)	RE	FT age	N	L	SD
Quercy/Rouergue																		
MC20	Lieucamp	tonalite	2.099	44.533	355	22	1.866	1433	1.826	1402	6.515	9715	92.2	0	118±5	-	-	-
MC21	Naussac	tonalite	2.105	44.521	236	18	3.295	1499	2.881	1311	6.564	9715	90.6	0	133±6	101	12.5±0.2	1.8
MC23	Galgan	granite	2.149	44.496	412	23	0.955	769	1.057	851	6.614	9715	46.8	5.1	106±6	-	-	-
MC19	La Peyrière	leucogranite	2.183	44.317	680	13	2.67	569	4.41	942	1.22	6787	14	10.9	123±8	100	13.6±0.1	1.30
Mount Lozère																		
MC24	Les Bondons	granite	3.628	44.381	878	19	3.998	1987	3.644	1811	5.654	5495	40.4	4.3	111±5	100	13.1±0.1	1.1
MC25	La Fage	granite	3.597	44.421	1157	19	3.217	1660	3.624	1870	5.585	6495	42.8	1.6	88±4	100	13.4±0.1	1.0
MC26	Frayssinet	granite	3.692	44.379	1001	22	0.850	568	1.121	749	5.495	5495	67.0	0.4	74±5	32	12.7±0.2	1.0
MC30	Miral	granite	3.692	44.364	760	22	0.760	703	0.906	838	5.487	5479	98.1	0	82±5	40	13.0±0.2	1.2
MC31	L'Aubaret	granite	3.833	44.352	1244	25	1.072	1002	1.059	990	5.416	5495	97.5	0.1	98±5	26	12.7±0.2	1.1
MC32	Pré de la Dame	granite	3.906	44.386	1469	24	0.706	970	0.740	1016	5.484	5479	43.4	6.2	90±5	87	12.9±0.1	1.0
MC36	Grattegals	lamprophyre	3.588	44.275	613	22	1.159	1113	0.752	722	5.336	5495	92.0	0	146±8	77	12.2±0.2	1.3
Margeride																		
MC39	Le Pin	granite	3.483	44.867	1150	20	5.81	2824	6.03	2931	1.140	7813	<1	10.3	183±8	104	11.8±0.3	3.1
MC40	St Alban	granite	3.400	44.800	1000	20	5.72	2236	5.83	2280	1.13	7813	10	5.5	186±6	101	11.5±0.3	2.6
MC41	Serverette	granite	3.383	44.717	992	20	5.15	1949	5.2	1967	1.130	7813	15	2.1	187±6	111	12.1±0.2	2.0
MC42	Can la Roche pass	granite	3.483	44.600	1000	20	6.980	2583	7.65	2832	1.23	7813	<1	8.5	170±6	100	11.7±0.3	2.8
MC43	Langogne	foliated granite	3.867	44.700	920	20	2.26	1430	3.85	2441	1.22	6787	12	7.7	121±5	100	13.4±0.2	1.5
MC38	Allenc	granite	3.67	44.55	1118	20	4.61	2006	4.3	1871	5.85	2924	78.7	0.1	112±5	100	13.4±0.1	1.2
MC44	Monistrol	porphyroïd granit	3.617	44.967	682	20	2.73	2033	5.48	4082	1.22	6787	0	13.9	102±4	100	13.3±0.1	1.3
MC45	Le Monastier	granite	4.017	44.933	926	20	3.570	1603	5.19	2332	1.13	7813	20	3.5	130±5	100	13.6±0.2	1.6
MC46	Alleyras	gneiss	3.700	44.917	950	20	2.27	1540	4.25	2879	1.12	7813	60	0.38	101±3	102	13.1±0.2	1.8

Table 3

	weight (µg)	Rs	FT	He (nccSTP/g)	U	Th	Sm	eU	Th/U	Age (Ma)	± 1s	Corrected Age Ma) *	± 1s
MCF20A	2.82	61.7	0.77	335176	28.1	16.0	15.1	32	0.6	86.7	6.9	112.5	9.0
MCF20B	7.29	86.8	0.83	501602	42.6	2.3	9.8	43	0.1	95.9	7.7	114.8	9.2
MCF20C	33.57	135.0	0.89	683675	36.1	14.7	17.7	40	0.4	142.2	11.4	159.1	12.7
MCF20D	1.60	48.4	0.71	255876	26.1	17.6	9.6	30	0.7	69.7	5.6	98.0	7.8
MCF20E	1.36	51.2	0.73	484961	44.2	8.1	11.0	46	0.2	86.8	6.9	119.5	9.6
MCF23A	0.49	34.2	0.60	194855	15.8	24.3	38.3	22	1.5	73.8	5.9	122.4	9.8
MCF23D	2.80	49.7	0.73	309989	24.6	29.9	55.3	32	1.2	79.8	6.4	109.9	8.8
MCF23E	0.61	39.1	0.65	287989	18.4	11.5	35.6	21	0.6	111.1	8.9	172.2	13.8
MCF25	3.14	54.3	0.787	294268	219	15	643	223	0.1	107	8.6	134	9
MCF25A	2.61	61.8	0.77	923122	58.7	6.4	30.0	60	0.1	126.3	10.1	163.6	13.1
MCF25B	5.24	68.8	0.79	822675	66.9	5.5	38.4	68	0.1	99.2	7.9	125.2	10.0
MCF25C	12.22	100.8	0.86	1281951	65.8	4.3	36.5	67	0.1	157.9	12.6	184.1	14.7
MCF25D	2.96	64.2	0.78	767762	54.6	7.1	32.2	56	0.1	112.3	9.0	144.0	11.5
MCF25E	2.28	62.0	0.77	1324232	81.2	17.2	40.1	85	0.2	127.9	10.2	166.0	13.3
MCF26	0.74	33.6	0.669	154185	79	66	511	94	0.84	58	4.6	87	6
MCF26AA	1.18	39.3	0.708	72021	67	58	534	81	0.9	70	5.6	87	6
MCF26BB	2.44	49.5	0.756	37591	35	53	607	48	1.5	59	4.7	74	5
MCF26B	1.58	46.9	0.70	306855	32.0	31.1	70.1	40	1.0	63.5	5.1	90.4	7.2
MCF26F	2.17	53.7	0.74	224487	15.8	25.3	45.7	22	1.6	83.7	6.7	113.3	9.1
MCF31A	1.38	39.5	0.662	38071	15	16	190	19	1.05	69	5.5	104	7
MCF31AA	2.69	46.2	0.719	92048	41	48	210	53	1.16	63	5.0	87	6
MCF31BB	2.17	45.7	0.726	73888	73	75	581	91	1.0	64	5.1	80	6
MCF31B	0.85	36.7	0.63	385316	41.8	51.9	74.5	54	1.2	58.3	4.7	92.7	7.4
MCF31C	0.90	38.1	0.64	152715	20.3	41.3	53.5	30	2.0	41.4	3.3	64.9	5.2
MCF31D	0.76	34.9	0.61	156440	22.1	40.5	57.5	32	1.8	40.2	3.2	66.1	5.3
MCF31F	1.42	45.3	0.69	152547	16.9	39.8	58.8	26	2.4	47.1	3.8	68.0	5.4
MCF31G	1.23	38.7	0.65	289364	34.2	39.8	65.0	44	1.2	54.2	4.3	83.9	6.7
MCF31H	1.83	54.0	0.74	154055	11.3	31.9	56.4	19	2.8	66.1	5.3	89.5	7.2
MCF36A	7.49	76.4	0.813	71835	17	21	93	22	1.27	117	9.4	144	10
MCF36B	6.94	70	0.821	51746	13	32	103	20	2.56	91	7.3	110	8
MCF36C	6.02	60.5	0.801	62592	12	29	108	19	2.44	118	9.4	146	10
MCF36D	2.15	50.3	0.715	75228	39	84	653	59	2.2	97	7.8	121	8
MCF36E	1.90	56.9	0.75	313125	10.7	35.7	36.7	19	3.3	133.5	10.7	177.6	14.2
MCF36F	3.07	54.6	0.74	390872	17.4	48.5	54.7	29	2.8	110.3	8.8	149.0	11.9
MCF36G	3.38	56.6	0.75	403821	16.1	40.0	52.5	26	2.5	128.6	10.3	170.9	13.7
MCF38A	2.90	55.3	0.75	1594546	106.1	14.7	38.6	110	0.1	120.0	9.6	161.0	12.9
MCF38B	2.90	55.3	0.75	1465361	112.7	16.9	40.3	117	0.1	103.5	8.3	138.7	11.1
MCF38C	2.24	62.4	0.77	1724954	142.7	12.5	37.6	146	0.1	97.7	7.8	126.5	10.1
MCF38D	7.83	76.9	0.81	1243249	88.7	18.1	30.7	93	0.2	110.3	8.8	135.4	10.8
MCF38E	2.44	53.9	0.74	2183937	139.2	10.8	43.9	142	0.1	127.0	10.2	171.7	13.7

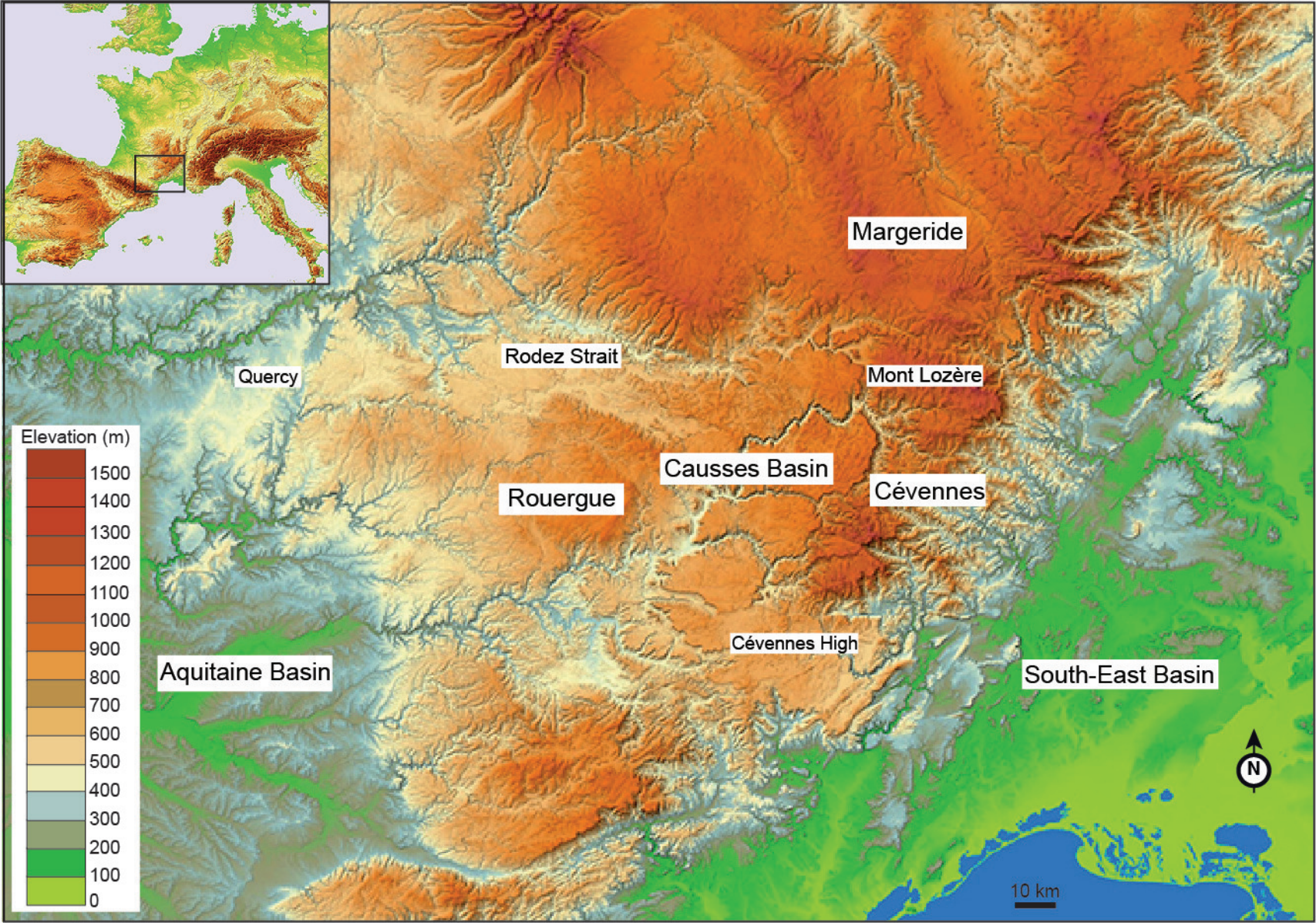
Margeride
Rodez Strait
Quercy
Mont Lozère
Causses Basin
Cévennes
Rouergue
Cévennes High
Aquitaine Basin
South-East Basin
Elevation (m)
1500
1400
1300
1200
1100
1000
900
800
700
600
500
400
300
200
100
0
N
10 km

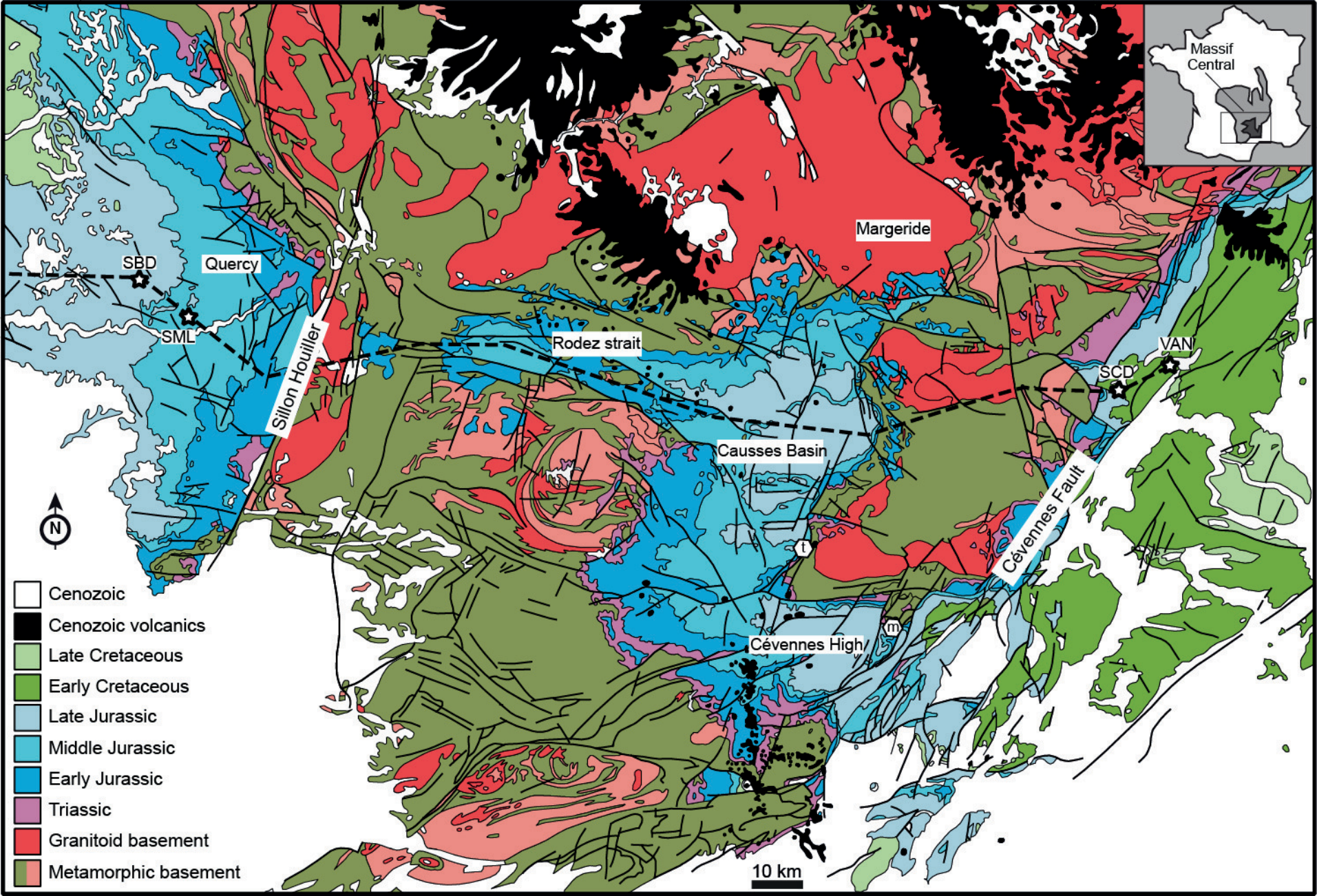
Massif Central
Margeride
SBD
Quercy
SML
Sillon Houiller
Rodez strait
VAN
SCD
Causses Basin
Cévennes Fault
t
m
Cévennes High
N
Cenozoic
Cenozoic volcanics
Late Cretaceous
Early Cretaceous
Late Jurassic
Middle Jurassic
Early Jurassic
Triassic
Granitoid basement
Metamorphic basement
10 km

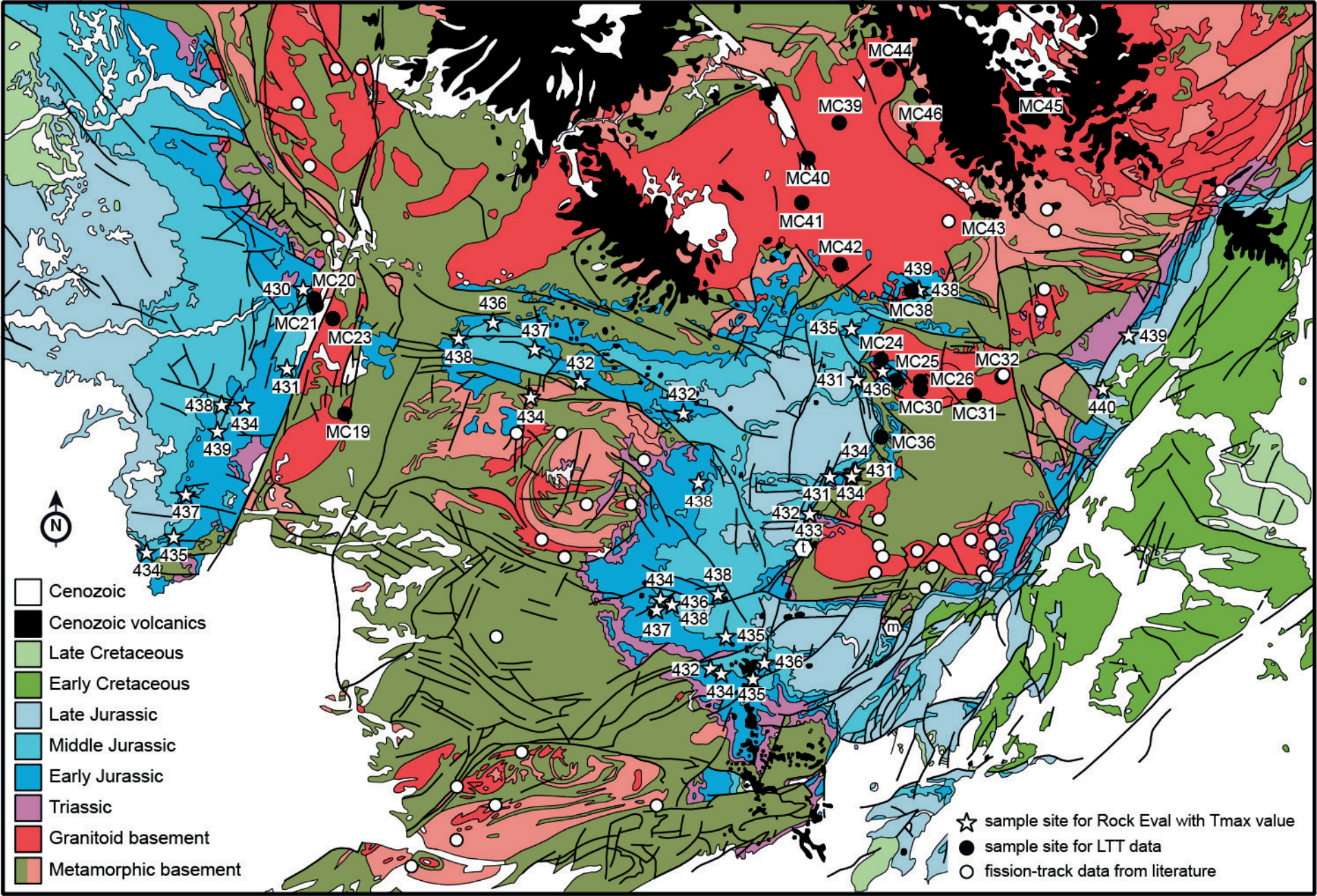
MC44
MC39
MC46
MC45
MC40
MC41
MC43
MC42
439
438
MC38
MC20
430
436
MC21
437
MC23
435
MC24
MC25
MC32
438
432
431
MC26
436
439
432
MC30
MC31
440
438
434
434
MC19
MC36
439
434
431
437
438
431
434
432
433
435
434
438
434
436
438
437
435
436
432
434
435
Cenozoic
Cenozoic volcanics
Late Cretaceous
Early Cretaceous
Late Jurassic
Middle Jurassic
Early Jurassic
Triassic
Granitoid basement
Metamorphic basement
sample site for Rock Eval with Tmax value
sample site for LTT data
fission-track data from literature

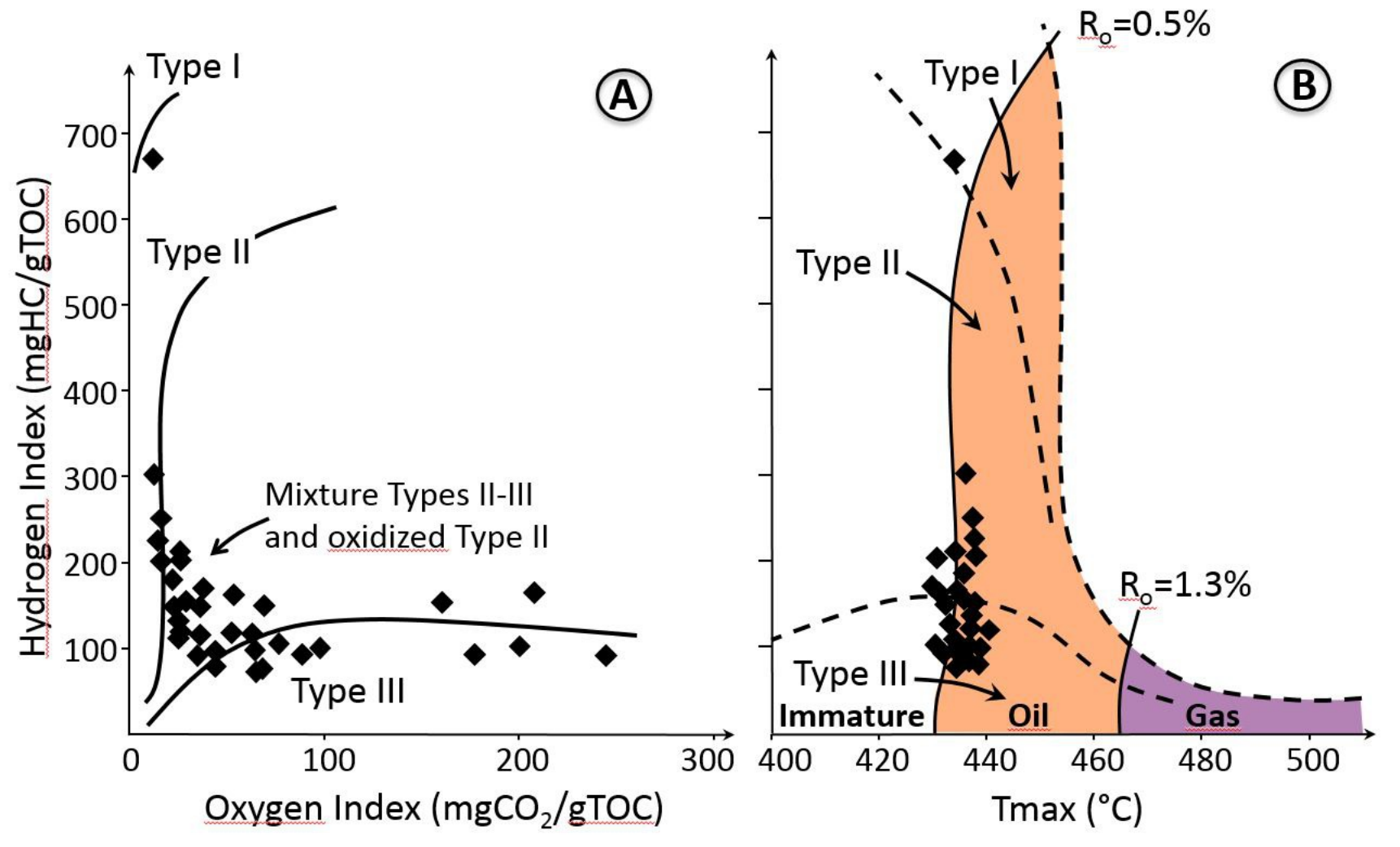
A
Type I
Type II
Mixture Types II-III
and oxidized Type II
Type III
Hydrogen Index (mgHC/gTOC)
700
600
500
400
300
200
100
0
100
200
300
Oxygen Index (mgCO2/gTOC)
B
Ro=0.5%
Type I
Type II
Ro=1.3%
Type III
Immature
Oil
Gas
400
420
440
460
480
500
Tmax (°C)

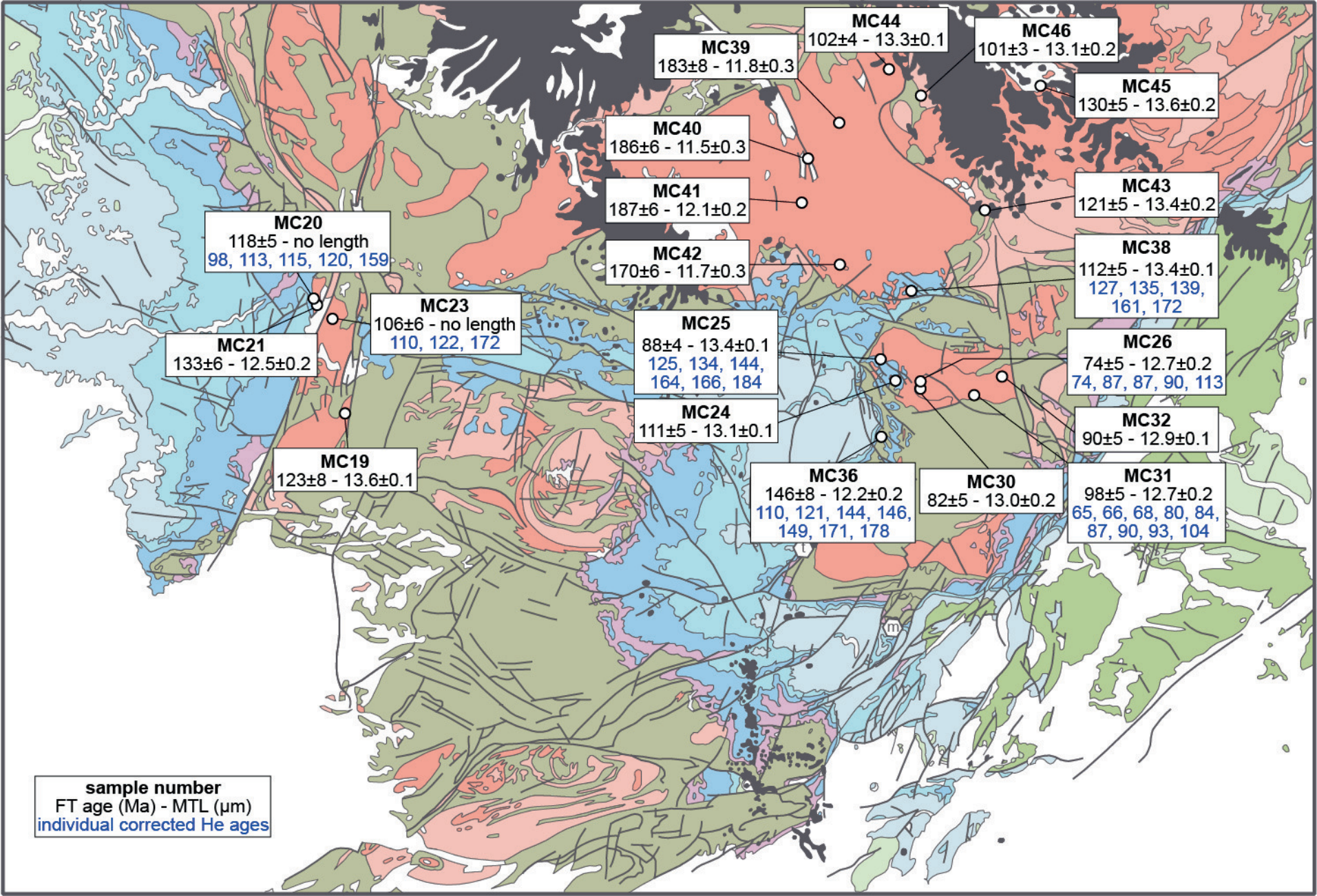
MC44
102±4 - 13.3±0.1
MC46
101±3 - 13.1±0.2
MC39
183±8 - 11.8±0.3
MC45
130±5 - 13.6±0.2
MC40
186±6 - 11.5±0.3
MC41
187±6 - 12.1±0.2
MC43
121±5 - 13.4±0.2
MC20
118±5 - no length
98, 113, 115, 120, 159
MC42
170±6 - 11.7±0.3
MC38
112±5 - 13.4±0.1
127, 135, 139,
161, 172
MC23
106±6 - no length
110, 122, 172
MC25
88±4 - 13.4±0.1
125, 134, 144,
164, 166, 184
MC21
133±6 - 12.5±0.2
MC26
74±5 - 12.7±0.2
74, 87, 87, 90, 113
MC24
111±5 - 13.1±0.1
MC32
90±5 - 12.9±0.1
MC19
123±8 - 13.6±0.1
MC36
146±8 - 12.2±0.2
110, 121, 144, 146,
149, 171, 178
MC30
82±5 - 13.0±0.2
MC31
98±5 - 12.7±0.2
65, 66, 68, 80, 84,
87, 90, 93, 104
sample number
FT age (Ma) - MTL (µm)
individual corrected He ages

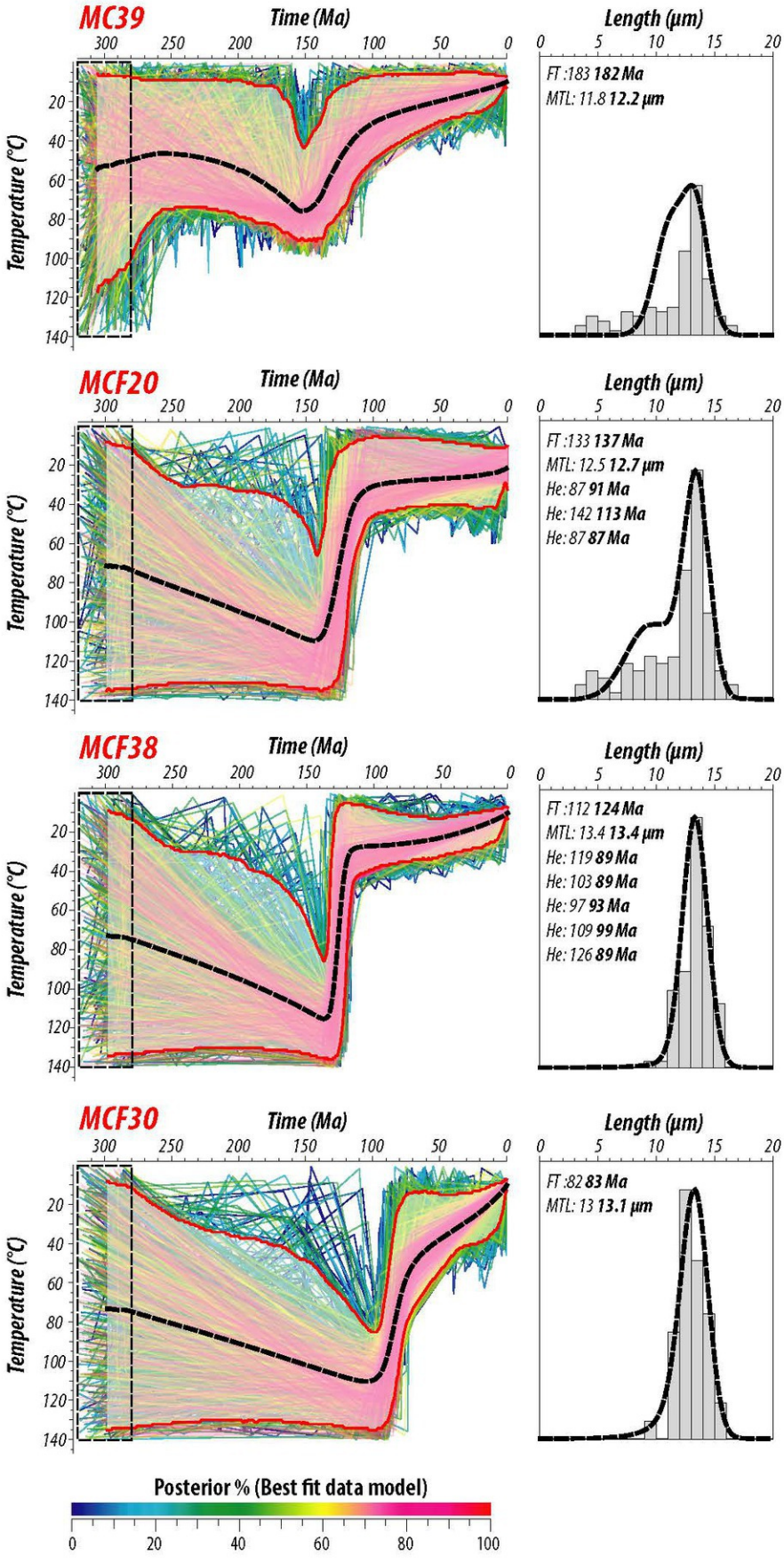
MC39
Time (Ma)
Length (μm)
Temperature (°C)
FT :183 182 Ma
MTL: 11.8 12.2 μm
MCF20
Time (Ma)
Length (μm)
Temperature (°C)
FT :133 137 Ma
MTL: 12.5 12.7 μm
He: 87 91 Ma
He: 142 113 Ma
He: 87 87 Ma
MCF38
Time (Ma)
Length (μm)
Temperature (°C)
FT :112 124 Ma
MTL: 13.4 13.4 μm
He: 119 89 Ma
He: 103 89 Ma
He: 97 93 Ma
He: 109 99 Ma
He: 126 89 Ma
MCF30
Time (Ma)
Length (μm)
Temperature (°C)
FT :82 83 Ma
MTL: 13 13.1 μm
Posterior % (Best fit data model)

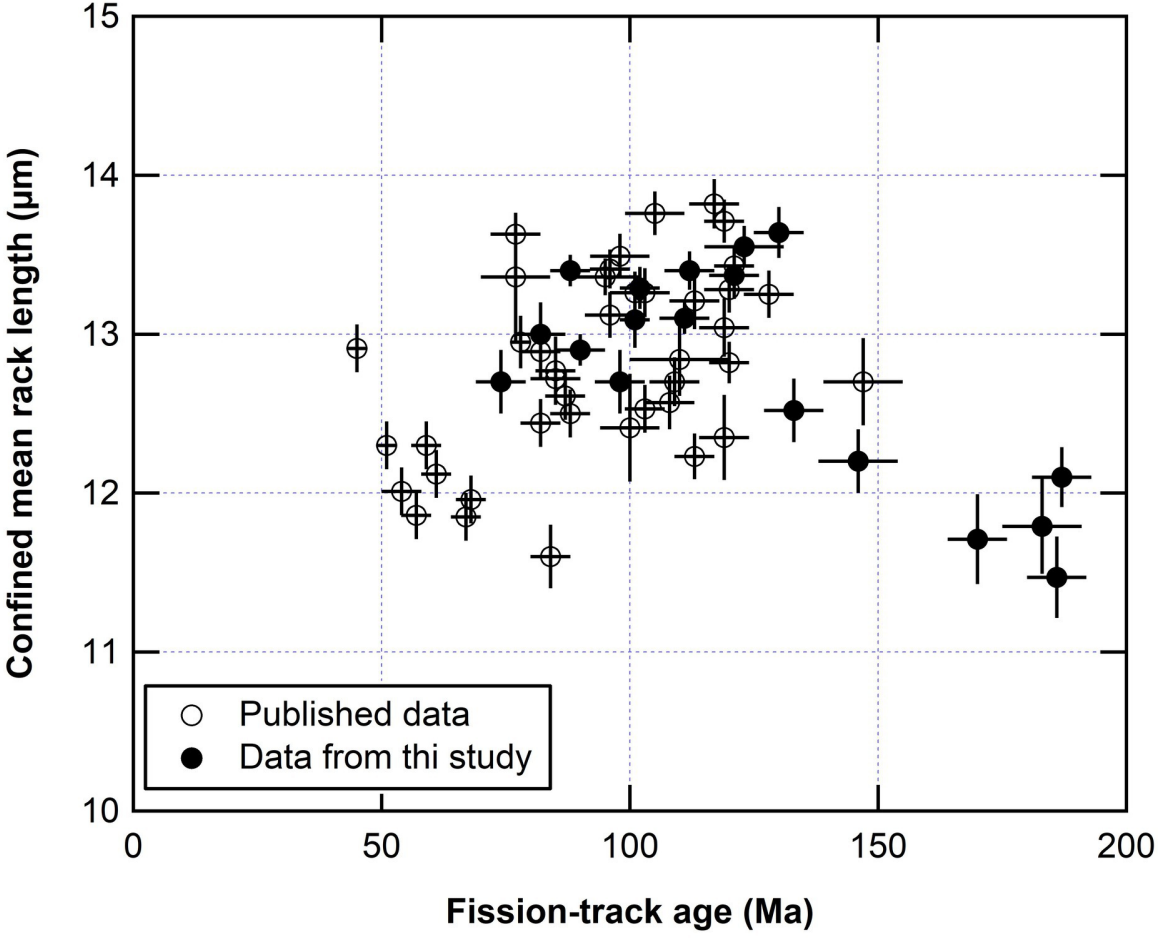
Confined mean rack length (μm)
15
14
13
12
11
10
0
50
100
150
200
Fission-track age (Ma)
Published data
Data from thi study

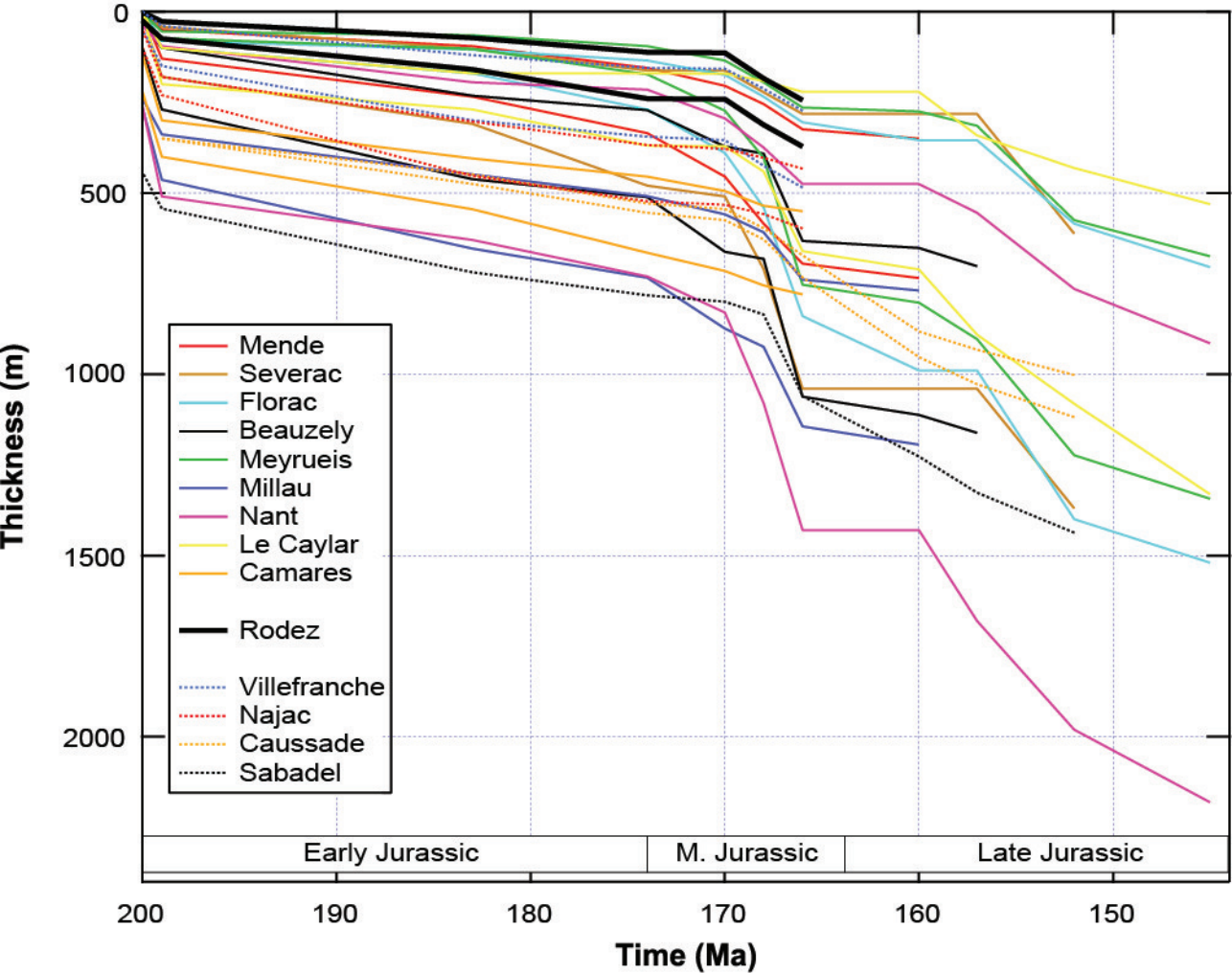
Thickness (m)
0
500
1000
1500
2000
Mende
Severac
Florac
Beauzely
Meyrueis
Millau
Nant
Le Caylar
Camares
Rodez
Villefranche
Najac
Caussade
Sabadel
Early Jurassic
M. Jurassic
Late Jurassic
200
190
180
170
160
150
Time (Ma)

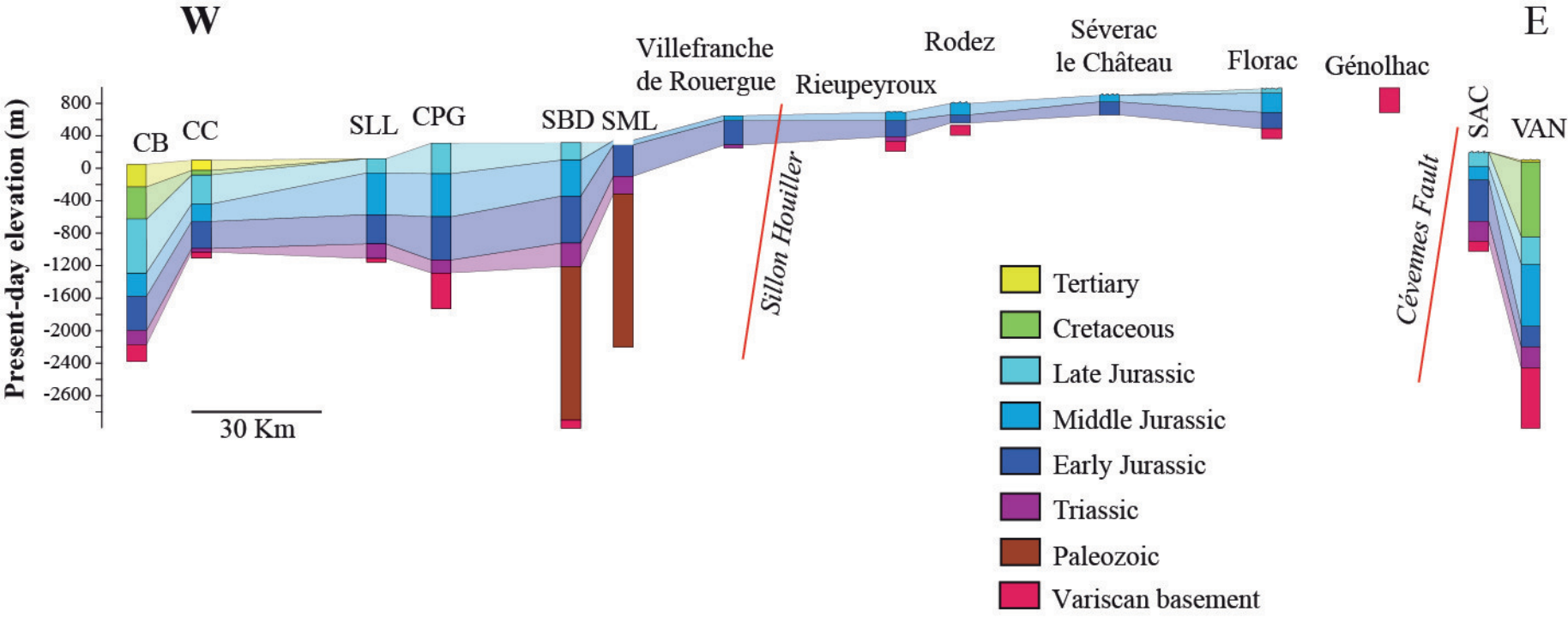
W
E
Present-day elevation (m)
800
400
0
-400
-800
-1200
-1600
-2000
-2400
-2600
CB
CC
SLL
CPG
SBD
SML
Villefranche
de Rouergue
Rieupeyroux
Rodez
Séverac
le Château
Florac
Génolhac
SAC
VAN
Sillon Houiller
Cévennes Fault
30 Km
Tertiary
Cretaceous
Late Jurassic
Middle Jurassic
Early Jurassic
Triassic
Paleozoic
Variscan basement

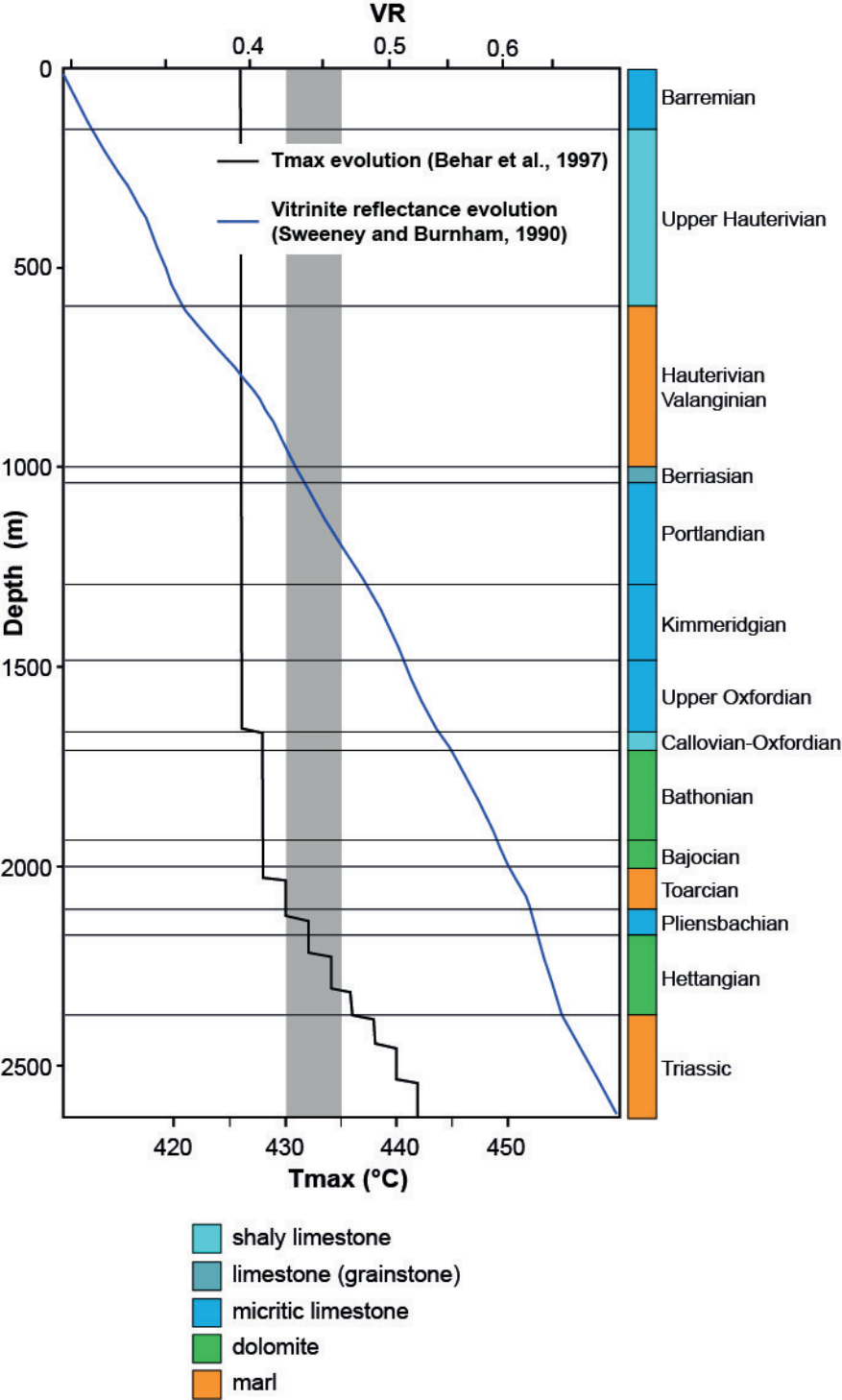
VR
0.4
0.5
0.6
0
500
1000
1500
2000
2500
Depth (m)
Tmax evolution (Behar et al., 1997)
Vitrinite reflectance evolution
(Sweeney and Burnham, 1990)
Barremian
Upper Hauterivian
Hauterivian
Valanginian
Berriasian
Portlandian
Kimmeridgian
Upper Oxfordian
Callovian-Oxfordian
Bathonian
Bajocian
Toarcian
Pliensbachian
Hettangian
Triassic
420
430
440
450
Tmax (°C)
shaly limestone
limestone (grainstone)
micritic limestone
dolomite
marl

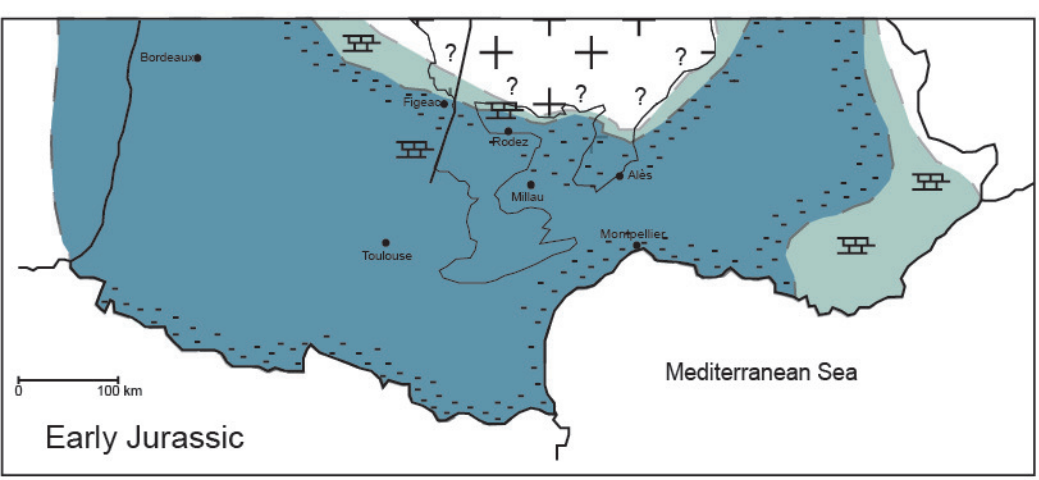
Bordeaux
Figeac
Rodez
Alès
Millau
Montpellier
Toulouse
Mediterranean Sea
0
100 km
Early Jurassic

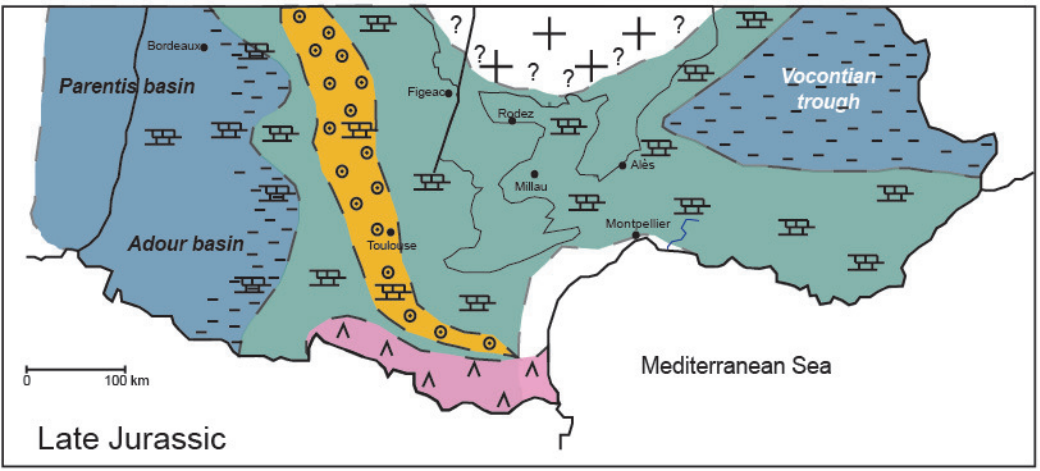
Bordeaux
Parentis basin
Adour basin
Figeac
Rodez
Alès
Millau
Montpellier
Toulouse
Vocontian trough
Mediterranean Sea
0
100 km
Late Jurassic

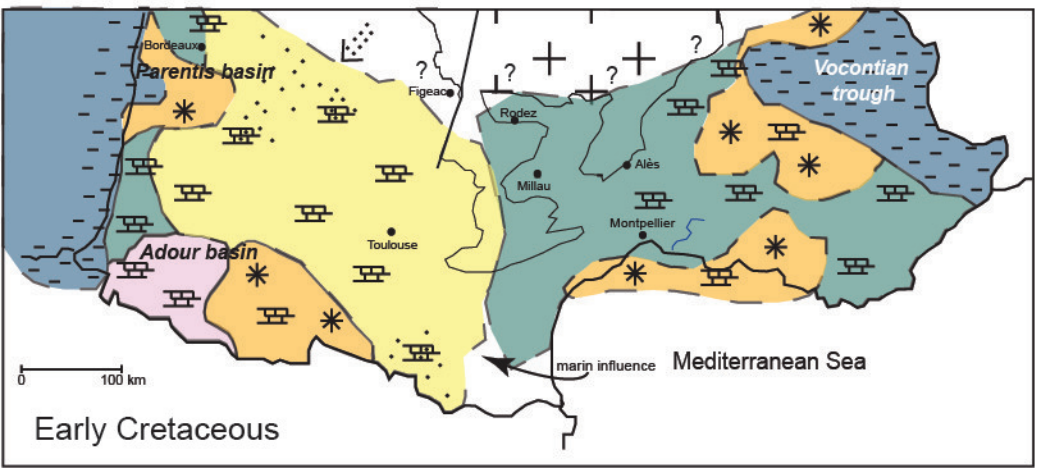
Bordeaux
Parentis basin
Adour basin
Figeac
Rodez
Alès
Millau
Montpellier
Toulouse
Vocontian trough
marin influence
Mediterranean Sea
0
100 km
Early Cretaceous

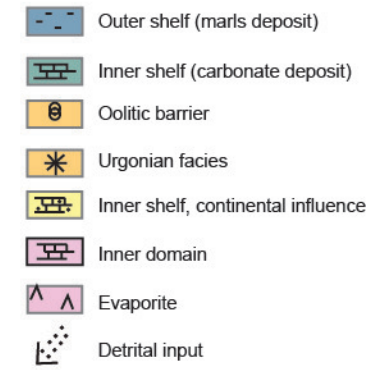
Outer shelf (marls deposit)
Inner shelf (carbonate deposit)
Oolitic barrier
Urgonian facies
Inner shelf, continental influence
Inner domain
Evaporite
Detrital input